

GRS 1915+105 and the Disc-Jet Coupling in Accreting Black Hole Systems

Rob Fender

Astronomical Institute Anton Pannekoek, University of Amsterdam, Kruislaan 403, 1098 SJ Amsterdam,
The Netherlands

Tomaso Belloni

INAF—Osservatorio Astronomico di Brera, Via E. Bianchi 46, I-23807 Merate, Italy

KEYWORDS: accretion, accretion disks, black hole physics, ISM: jets and outflows, X-rays:binaries,
radio continuum:stars

ABSTRACT: GRS 1915+105—the first stellar-scale, highly relativistic jet source identified—is a key system for our understanding of the disc-jet coupling in accreting black hole systems. Comprehending the coupling between inflow and outflow in this source is important not only for X-ray binary systems but has a broader relevance for studies of active galactic nuclei and gamma-ray bursts. In this paper, we present a detailed review of the observational properties of the system, as established in the decade since its discovery. We attempt to place it in context by a detailed comparison with other sources, and construct a simple model for the disc-jet coupling, which may be more widely applicable to accreting black hole systems.

CONTENTS

Introduction	2
GRS 1915+105	4
<i>Discovery and Early Observations</i>	4
<i>X-Ray Spectral Variability</i>	4
<i>Radio and Infrared Emission</i>	14
<i>Radio and Infrared Evidence for Disc-Jet Coupling</i>	20
Other Sources: GRS 1915+105 in Context	24
<i>Black Hole X-ray Binary States</i>	24
<i>GRS 1915+105 A/B/C States and Other Systems</i>	26
<i>Active Galactic Nuclei</i>	27
Interpretation: Many Flavors of Disc-Jet Coupling or Just One?	28
<i>Hard States and Jet Formation</i>	28
<i>On the Trigger of Optically Thin Events</i>	29
<i>Jet Power and Velocity</i>	30
<i>A Unified (Toy) Model of Disc-Jet Coupling</i>	31
Conclusions	34

1 Introduction

Jets—highly relativistic, collimated, powerful outflows—seem to be an almost ubiquitous feature of accreting black holes, and yet remain poorly understood. Widely studied in active galactic nuclei (AGN), their association with the coupled process of accretion has been obstructed by the long dynamical timescales associated with these objects. How matter falling at high speed toward a black hole

manages to escape to the external universe remains a mystery ¹ that can only be solved by studying the coupled processes of inflow and outflow. The key to this puzzle seems to lie with binary systems in our own galaxy, which harbor stellar-mass (5–15 M_{\odot}) black holes that—we are just beginning to appreciate—seem to display the same kind of inflow:outflow coupling as AGN but on timescales typically six to eight orders of magnitude shorter in proportion to M . Thus, although AGN are the powerhouses of the universe, it is their nearby cousins, which vary rapidly enough that humans may follow the changes in the disc-jet coupling, to which we turn for an understanding of the relation between accretion and jets around black holes.

With the launch of the *Rossi X-Ray Timing* satellite (*RXTE*), an unprecedented wealth of X-ray data from black hole candidates (BHC) has become available to the astronomical community. In particular, several bright transient systems have been followed with a large number of densely packed observations (see McClintock & Remillard 2004). These observations have increased our knowledge of the high-energy properties of these systems, although we still do not have a complete picture of the physical mechanisms underlying the X-ray emission.

GRS 1915+105, a binary system in our galaxy containing an accreting black hole of probable mass $\sim 15M_{\odot}$, is a key object for the study of the disc-jet connection. Its peculiar X-ray properties, coupled with other characteristics in common with other systems, allow us to study in detail the instabilities of the accreting gas. These instabilities have been positively associated with the ejection of relativistic jets and to related flaring episodes in the radio band. This means that the interaction of emitted powerful collimated jets can be studied on different timescales and associated with (near-)simultaneous events in the accretion flow that provides the gas for them. The uniqueness of GRS 1915+105 stimulated us to center a full discussion on the disc-jet coupling on this system.

The review is structured as follows: In Section 2, the X-ray and radio properties of GRS 1915+105 are described, followed by the disc-jet coupling evidences in this system. In Section 3, we describe other BHCs in a similar fashion, whereas in Section 4, we concentrate on discussing the comparison between all systems. Our main conclusions are presented in Section 5.

¹To quote Krolik (1999), “In principle one could imagine that accretion onto a black hole occurs without any outflow at any point. Put another way, we do not know why jets exist.”

2 GRS 1915+105

2.1 *Discovery and Early Observations*

GRS 1915+105 was discovered on August 15, 2002, with the WATCH instrument on board *GRANAT* as a 300 mCrab transient (Castro-Tirado et al. 1992, 1994) and immediately detected at higher energies by *CGRO*/BATSE (Harmon et al. 1992). A time-variable radio counterpart (Mirabel et al. 1993a) and an IR counterpart (Castro-Tirado et al. 1993, Mirabel et al. 1993b) were discovered in the ROSAT HRI error box (Greiner 1993). The X-ray spectrum appeared to be variable and two-component (see, e.g., Alexandrovich et al. 1994). *GRANAT*/WATCH and *CGRO*/BATSE monitoring of the source showed periods of nondetection but never simultaneously in both instruments, indicating that GRS 1915+105 was continuing the same outburst started in 1992 (see Zhang et al. 1995, Sazonov & Sunyaev 1995, Paciesas et al. 1996, Harmon et al. 1997). A BATSE hard X-ray light curve extending up to the beginning of 1996 can be seen in Figure 1. Paciesas et al. (1996) realized that the source was showing an unusual level of variability, although the true uniqueness of its nature was not clear from those data. The radio counterpart of GRS 1915+105 was observed to be variable in flux and spectrum (see Rodríguez & Mirabel 1993), and the radio variability was correlated to the hard X-ray flux (Mirabel et al. 1994). The major breakthrough took place when Mirabel & Rodríguez (1994) used the VLA radio to observe components moving away from GRS 1915+105 with apparent superluminal velocity, at the same time estimating a distance of 12.5 kpc (see Rodríguez et al. 1995), which excluded an extragalactic origin. GRS 1915+105 became the first superluminal source in our Galaxy (see Section 2.3.1).

2.2 *X-Ray Spectral Variability*

The launch of *RXTE* opened a new window to GRS 1915+105. The large area of the proportional counter array (PCA) (Jahoda et al. 1996), the broad-band coverage provided by the High-Energy X-ray Timing Experiment (HEXTE) instrument (Rothschild et al. 1998), the monitoring capabilities of the All-Sky Monitor (ASM) (Levine et al. 1996), and the extreme flexibility of scheduling and pointing were key factors that allowed a more complete view of the unique X-ray properties of this system. The full ASM light curve from the start of the *RXTE* mission to October 12, 2003, averaged over one-day bins, can be seen in Figure 2. These data start just after the time window of the BATSE data in Figure 1. From Figure 2, the peculiarity of the variability of GRS 1915+105 on timescales longer than one day is evident. Greiner et al. (1996) were the first to

report an unusual level of X-ray variability in GRS 1915+105 on timescales of subseconds to days. The light curves presented in that work were complex and structured in a way that was never observed before in any X-ray source. The authors attributed this variability to the effect of a major accretion disc instability and argued that major events like those shown in Figure 3 could be related to radio flares observed later. A classification of spectral/timing patterns from early *RXTE*/PCA data was presented by Chen et al. (1997), who identified two spectral states: a hard one with a strong 0.5–6.0 Hz quasi-periodic oscillations (QPOs), and a soft one with no QPOs (see also Paul et al. 1997). In the same year, Belloni et al. (1997a) accumulated PCA energy spectra from the high-flux and low-flux intervals seen in Figure 3 and fitted them with the “standard” simplified model for BHCs, consisting of a disc-blackbody component (see Mitsuda et al. 1984) plus a power-law component to account for the high-energy tail. The free parameters of this model are the flux F_{pl} and photon index Γ of the power-law and the inner radius of the accretion disc R_{in} and temperature at the inner radius T_{in} . The strong and sudden hardening events seen in the hardness curve in Figure 3 can then be understood in terms of a hardening (from $\Gamma \sim 3.6$ to $\Gamma \sim 2.2$) of the power law and a softening ($kT_{in} \sim 2.2$ to ~ 0.6 keV) of the disc component. At the same time, the inner-disc radius R_{in} , which in many sources had been observed to remain constant at a value of a few dozen kilometers (interpreted as the innermost stable orbit, see Tanaka & Lewin 1995; see below) was seen to increase from ~ 20 to ~ 300 km. The interpretation of these transitions, which happened on a timescale of a few seconds, was that they were due to the onset of a thermal-viscous instability. In this framework, the sudden increase in R_{in} corresponded to the inner portion of the accretion disc becoming unobservable in the X-ray band. The accreting matter passing through R_{in} would slowly “refill” the unobservable region on a viscous timescale, increasing the surface density of the inner portion of the disc until the reverse transition would take place and go back to a fully observable disc. In this interpretation, it is not necessary that the inner part of the disc is completely emptied of gas, but simply that the gas makes a transition to a much cooler state, which makes it effectively invisible in X-rays.

This picture was subsequently strengthened by the analysis of more observations (Belloni et al. 1997b). Time-resolved spectroscopy allowed the evolution of the spectral parameters to be followed in detail (see Figure 4). In particular, Belloni et al. (1997b) found that in the soft intervals, R_{in} was approximately constant around 20 km, independent of the length of the interval, whereas in the hard intervals, the radius showed a time evolution. The maximum radius reached in each hard interval was strongly correlated with the length of the interval t_{hard} (see Figure 5) and anticorrelated with the minimum flux reached. In the framework of the instability picture of Belloni et al. (1997a), this has a direct

interpretation: The spectral evolution and the duration of the event are determined by one parameter only, namely, the radius of the missing inner section of the accretion disc, i.e., R_{in} . For a large radius, the drop in flux will be large and the time needed for refill will be long. Associating the refill time with the disc viscous timescale t_{visc} at R_{in} , can be expressed as

$$t_{visc} = 30\alpha_{-2}^{-1}M_1^{-1/2}R_7^{7/2}\dot{M}_{18}^{-2}\text{ s}, \quad (1)$$

where $\alpha_{-2} = \alpha/0.01$, R_7 is the radius in units of 10^7cm , M_1 is the black hole mass in solar masses, and \dot{M}_{18} is the accretion rate in units of 10^{18} g/s (see Belloni et al. 1997b). From this, under the reasonable assumption that the external \dot{M} does not vary within a one-hour observation, we expect to observe

$$t_{hard} \propto R_{in}^{7/2}. \quad (2)$$

The line in Figure 5 shows a fit of t_{hard} versus R_{in} with a $y = x^{3.5}$ relation: Only the longest interval deviates from the expected relation. The two quantities t_{hard} and R_{in} are determined in a completely different fashion, the first from timing analysis and the second from a spectral decomposition, ensuring that the observed correlation is not spurious. The relation in Figure 5 is a direct measurement of the radial dependence of a fundamental quantity of an accretion disc, obtained through the analysis of the variability from a source that is indeed peculiar, but also shows many properties in common with other systems. Owing to the approximations in the disc blackbody model, the measurement of the inner-disc radius cannot be considered precise in its absolute value (see Merloni et al. 2000), although large variations, such as those observed in GRS 1915+105, cannot be due to these approximations. From this observation, a one-to-one correlation between the length of an instability interval and the following high-rate interval was found. Yadav et al. (1999) found that indeed in many observations made with the *IXAE* satellite, the length of the instability interval correlated with the length of the following high-rate interval and not with that of the preceding one. Therefore, the full observed high-low cycles are caused by the onset of the instability, which is not directly influenced by the duration of the “stable” interval.

2.2.1 Classification and Source Spectral States

Markwardt et al. (1999), analyzing in detail a specific *RXTE*/PCA observation from 1997, identified three separate states on the basis of timing and spectral characteristics. Figure 6 shows the spectral characterization of these states in terms of power-law photon index and inner-disc temperature.

A complete classification of the light curves observed by *RXTE*/PCA from GRS 1915+105 during the first two years of the mission was presented by Belloni et al. (2000). The observed light curves were divided into 12 classes (shown in Figure 7) on the basis of their timing and color properties. These 12 classes, later increased to 13 by Klein-Wolt et al. (2002) and possibly to 14 by Hannikainen et al. (2003), are not meant to be exhaustive but as a starting point for subsequent analysis. From this classification and from a detailed analysis of X-ray color-color diagrams, Belloni et al. (2000) concluded that, as suggested by Markwardt et al. (1999) for a single observation, indeed the flux and spectral variability of GRS 1915+105 can be interpreted as transitions between three separate states. They called these states A, B, and C. Figure 8 shows a schematic view of the three states in terms of their X-ray colors:

- State A: softer spectrum, dominated by a disc component with $kT_{in} > 1$ keV. Mostly little time variability.
- State B: softer spectrum, dominated by a disc component with a larger temperature than state A. Substantial red-noise variability on timescales > 1 s.
- State C: hard colors, with the spectrum dominated by a relatively flat power-law ($\Gamma=1.8-2.5$). White noise variability on timescales > 1 s.

The transitions between these three states are so far observed only in the directions indicated by arrows in Figure 8, i.e., no direct $C \Rightarrow B$ are seen. These states connect to the instability picture outlined above in the following way: state C corresponds to the onset of the instability in the inner section of the disc, whereas states A and B correspond to stable periods. This means that the transitions that involve state A are not interpreted within that picture. The existence of definite events that cannot be interpreted in a thermal-viscous instability framework was already pointed out by Taam et al. (1997), who analyzed a *RXTE*/PCA observation of class ν . They showed that the difference between state A and state B can be associated to a variation in the inner edge of the accretion disc, although of smaller amplitude than that observed during state C. This picture is confirmed by a more complete analysis by Migliari & Belloni (2003).

An analysis of time-resolved spectra from a large number of *RXTE*/PCA observations, together with timing analysis, was made by Munro et al. (1999), who presented a number of correlations between spectral parameters and timing parameters. Vilhu & Nevalainen (1998) analyzed observations of class ρ and interpreted through spectral fitting that the regular “ring” in the color-color diagram is due to out-of-phase oscillations of different spectral parameters.

A full spectral analysis on a timescale of 16 s of the instability oscillations in class- β observations showed that indeed the inner-disc radius estimated from the disc blackbody component is larger during state A than during state B (Migliari &

Belloni 2003). Moreover, there is evidence for changes in the local accretion rate through the disc during states C and B but not during state A, where inner-disc temperature and radius change in a way that reflects a constant disc accretion rate (see Figure 9).

These results were followed by a series of theoretical papers aimed at a more thorough exploration of the connection with accretion disc models (Szuszkiewicz & Miller 1998, 2001; Nayakshin et al. 2000; Janiuk et al. 2000a,b; Nandi et al. 2001; Zampieri et al. 2001; Livio et al. 2003).

The complexity of the variability observed in GRS 1915+105 is unique and difficult to model. Clearly, it will not be possible to interpret in detail every aspect of the complex light curves shown in Figure 7, yet the structure of these light curves is not random and contains information about the accretion disc of GRS 1915+105. As can be seen from different works (e.g., Belloni 2001), there are complex light curves that repeat almost identically years apart. Although at first sight the X-ray light curves observed from GRS 1915+105 seem wildly different, the number of repetition patterns observed by *RXTE* in the past nine years of observations is relatively small, although clearly larger than 12. All the models listed in the previous paragraph are aimed at explaining the single A–B–C event and its appearing on different timescales, but the observed sequence of events is complex and by no means random. This aspect has not been investigated so far. For instance, Naik et al. (2002) found that certain variability classes are observed preferably before and after long C-state intervals (plateaux, see below), indicating a connection between the observed patterns and the long-term behavior, possibly linked to the mass accretion rate.

The issue of timescales deserves particular attention. As we have shown above, the length of C-state intervals observed within one PCA light curve can vary from a few seconds to half an hour. However, there are observations when the source is observed only in state C (defined as class χ in Belloni et al. 2000). Because each observation lasts typically one hour, it is reasonable to hypothesize that these are one-hour segments of longer state-C intervals. In some cases, this can be measured directly. From Figure 2, one can see intervals of relatively little variability in the daily ASM scans (for instance, around days 200 and 650), corresponding to a higher value of hardness ratio. These intervals have been called plateaux. In addition, a longer, lower, extended hard state is also visible in Figure 2, lasting more than a year and centered around day 400. The color properties of these plateaux have been analyzed by Belloni et al. (2000), who found that their properties are consistent with being long state-C intervals. This is confirmed also by timing analysis and by the radio properties (see below). A full spectral analysis of the long plateau was presented by Trudolyubov et al. (1999a), whereas Trudolyubov (2001) compared in detail the properties of these three plateaux and found that both spectral and timing characteristics differ

between the short plateaux and the long plateaux (see also Belloni et al. 2000). These differences are accompanied by marked differences in the radio emission (see below). Fast variations, probably associated with $B \leftrightarrow A$ state transitions, have also been observed in class μ and ρ (Taam et al. 1997, Belloni et al. 2000). They take place on a timescale as low as 0.1 s.

Such a complex light curve as the one shown in Figure 2 has of course been searched for patterns and periodicities. The problem is complex owing to the fact that single ASM scans, lasting a few seconds, sample complex behaviors, such as those in Figure 7, in a random way. A simple power density spectrum of this curve would not yield believable results. Different approaches were followed. Rau et al. (2003), on the basis of spectral analysis of class- χ observations only, detected a 590-day-long term periodicity in the power-law photon index, which they also observe in BATSE and radio data, possibly related to disc precession. Greenhough et al. (2003), through differencing and rescaling techniques that allowed them to separate different timescales, identify a 12–17 day timescale in the ASM light curve, which might be related to the binary orbital period of 35 days.

An obvious question to be answered is why this complex behavior is so unusual and has not been observed in any other sources. As shown below, both (fast) timing and spectral properties of this system are not at all peculiar. There is no definite answer as yet, although it is widely assumed that the large value of mass accretion rate (which, depending on the observation and on the spectral model, has been measured even to exceed the Eddington luminosity for a $14M_{\odot}$ object) plays a fundamental role in setting up these instabilities.

2.2.2 X-Ray Spectra

In this section, we describe in more detail the X-ray energy spectra that have been measured from GRS 1915+105 by different authors.

Broad-band spectra In the presence of strong variability on short timescales, it is not possible to accumulate energy spectra with sufficient statistics to test models more complicated than simple phenomenological approximations. Therefore, most of the efforts have been directed to the fitting and interpretation of data from observations with little variability.

Grove et al. (1998) reported *CGRO*/OSSE spectra (40 keV–10 MeV) of GRS 1915+105. In all three observations, a single power-law with no observable high-energy cutoff up to 500 keV was observed, unlike other BHCs in their low/hard state. OSSE observations span one or two weeks: For the two observations of 1996 and 1997 during this period, the *RXTE*/PCA database show observations of classes χ and μ in 1996 and of class α in 1997. This means that, although

different states were sampled by OSSE, GRS 1915+105 was probably in the C state for most of the time, when the power-law component is flatter. This was confirmed by Zdziarski et al. (2001), who analyzed a total of nine OSSE observations. The OSSE spectra, extending to 500 keV, do not show evidence of a high-energy cutoff. By checking the behavior of *RXTE*/PCA observations taken during the OSSE periods, they see that at least one of these observations consists probably of γ behavior dominated by state B. The conclusion is that no high-energy cutoff is seen in either state C or B (see Figure 10, color insert). The authors interpret this as evidence for the presence of a hybrid population of thermal and nonthermal electrons emitting through Comptonization and perform detailed joint *RXTE*/OSSE spectral fits. Assuming isotropic emission, the resulting bolometric luminosity is 6.5×10^{38} and 1.7×10^{39} erg/s for states C and B, respectively. For a black hole mass of $14M_{\odot}$, these values correspond to 0.35 and 0.93 of the Eddington luminosity. Evidence for only a thermal Comptonization component was presented by Vilhu et al. (2001) on the basis of a sample of *RXTE* spectra. These results are probably compatible, as the latter spectra did not extend to 500 keV as the OSSE ones did.

The issue of the presence/absence of a high-energy cutoff is not easy to solve. BeppoSAX spectra corresponding to both B and C states were analyzed by Feroci et al. (1999). The simultaneous 0.1–300 keV spectra were fitted with a multicolor disc, a cutoff-power-law, and a Compton reflection component. The reflection was rather large, with a value for $R = \Omega/2\pi$ of ~ 0.5 (where Ω is the solid angle subtended by the reflecting matter to the illuminating source). A definite high-energy cutoff was found for all observations, varying from 45 to 100 keV. Moreover, the cutoff energy was positively correlated with the power-law photon index. These results are clearly not compatible with the OSSE ones. PCA and HEXTE observations during the long plateau centered around day 400 in Figure 2 led to the detection of a high-energy cutoff whose value was rather constant around ~ 50 –100 keV (Trudolyubov et al. 1999a). The model adopted here was again a simplified multicolor disc plus cutoff-power-law. No correlation similar to the one reported by Feroci et al. (1999) was seen. As mentioned above, spectral analysis of PCA observations during the long plateaux and the shorter ones (days 200 and 650 in Figure 2), which are associated to different radio properties (see below), showed that the energy spectra are also different (Trudolyubov 2001). The shorter plateaux have a much lower cutoff energy, as low as 12–20 keV. This is in marked contrast with the OSSE results but is consistent with the results of the color analysis of Belloni et al. (2000). A simple phenomenological model consisting of a multicolor disc plus cutoff-power-law was used here again, to be compared with more complex physical models used to fit the *RXTE*+OSSE spectra, which, however, were not completely simultaneous given the length of the OSSE observations. Fits to class- χ PCA+HEXTE observations over the first four

years of *RXTE* by Rau & Greiner (2003) with a model consisting of a reflected power-law (plus disc), featuring no high-energy cutoff, yielded extremely high values for the reflection parameter R , inconsistent with other measurements.

It is clear that the different spectral models used are mostly responsible for the presence/absence of a high-energy cutoff. High signal-to-noise ratio simultaneous data are necessary to resolve the issue. The shape of the high-energy component also affects the measurements at lower energies, in particular, changing the normalization of the disc component, from which an estimate of the inner radius of the optically thick disc component can be extracted. Recent observations of GRS 1915+105 with INTEGRAL have been made and preliminary results are now available. A simultaneous *RXTE* and INTEGRAL observation during a plateau is reported by Fuchs et al. (2003b). Here the energy spectrum was fitted to a simple power-law up to 400 keV, with no reflection component nor high-energy cutoff (see Figure 11, color insert). Another INTEGRAL observation qualitatively confirms these results (Hannikainen et al. 2003).

Overall, the broad-band energy spectrum of GRS 1915+105 can be described in terms of three major components: a thermal component usually fitted with a multicolour disc-blackbody, a hard component fitted with either a simple power-law or a power-law with high-energy cutoff, or a more complex Comptonization model (with or without Compton reflection) and a emission line between 6 and 7 keV (see below). The relative contribution of these components varies on different states. The spectra discussed in this section are not different from those observed in other black hole systems.

Spectral Lines A series of observations with ASCA between 1994 and 1999 produced the first X-ray spectra with a resolution sufficiently high to explore narrow emission/absorption lines (Kotani et al. 2000). Absorption lines were detected and identified with resonant lines of calcium and iron, as well as blends of nickel and iron lines. Similar lines were observed only in the other superluminal source GRO J1655-40, and the authors speculated that they are associated to jet-production mechanisms. A 30-ks observation with the Chandra/HETGS (Lee et al. 2002) confirmed the presence of complex absorption structures, which were observed during a probable C state.

Although at a lower spectral resolution, a BeppoSAX spectrum taken in 1998 showed the clear presence of a broad emission line at 6.4 keV (Martocchia et al. 2002). The feature is broad and skewed, and fits with a relativistic model indicated a nonzero spin for the black hole in the system (see Figure 12). These observations corresponded to an interval when the line was particularly intense out of a series of long BeppoSAX exposures.

2.2.3 X-ray Timing

As in the case of energy spectra, the fast timing features of GRS 1915+105 are not as extraordinary as its variability on longer timescales. All observed properties in all three states appear rather normal, as they have been seen in a number of other BHCs (see McClintock & Remillard 2004). For a definition and description of the different components detected in the Fourier domain, see van der Klis (1995).

Noise and Low-Frequency Quasi-Periodic Oscillations Very complex power density spectra (PDS) have been presented by Morgan et al. (1997). Different continuum noise components and QPOs are visible in the PDS, although the production of one PDS per observation, without separating different intervals, makes it difficult to interpret the results. Three types of QPOs were identified: high-frequency (~ 70 Hz) oscillations (described below); low-frequency (1-10 Hz) QPOs (see also Paul et al. 1997); and very-low-frequency QPOs, which can be identified with the state transitions described above. A systematic difference between the PDS of soft and hard intervals was identified by Chen et al. (1997). On their hard branch (corresponding to state C, see above), the PDS of GRS 1915+105 consists of a flat-top noise component plus a 1–10 Hz QPO. The centroid frequency of the oscillation is well correlated with the count rate (see Figure 13) and shows higher harmonics that tend to disappear at high count rates. In their soft branch (states A and B), the PDS is steeper, with a broad peaked noise around 2 Hz. At high rates, selecting state B intervals during oscillations, the peaked noise disappears and a broad 5-Hz QPO peak appears (Chen et al. 1997). The three states identified by Markwardt et al. (1999) also have distinct timing characteristics corresponding to those of Chen et al. (1997).

As in the case of spectral analysis, most of the effort has been dedicated to the C state, which is relatively easier to analyze because of the long plateaux and the clear QPO at low frequencies (LFQPO). Markwardt et al. (1999) found that the LFQPO, like similar oscillations in other systems, has an energy spectrum consistent with that of the hard component, and that its centroid frequency correlates positively with the flux of the disc component (see also Muno et al. 1999). A correlation between the minimum centroid frequency reached during a C interval and the length of the interval (over a range of 5–500 s) was found by Trudolyubov et al. (1999b), who showed that in about half of the cases this correlation is consistent with the relation between viscous timescale at a certain radius and Keplerian frequency at the same radius. Rodriguez et al. (2002a,b) presented a combined spectral/timing analysis of PCA data, correlating the frequency of the QPO with the measured inner-disc radius, whereas a correlation with the power-law photon index was investigated by Vignarca et al. (2003). Many groups concentrated their work on the PCA observations of class χ , when

the source is always in state C. Many of these observations are parts of longer plateaux (see above). Trudolyubov et al. (1999a) analyzed PCA observations during the long radio-quiet plateau of 1996–1997 (around day 400 in Figure 2) and presented a number of correlations between timing and spectral parameters. A thorough work on timing analysis of PCA observations during both radio-loud and radio-quiet plateaux was done by Munro et al. (2001), who considered the correlation between radio and timing properties. Important differences in timing properties between radio-quiet and radio-loud plateaux, associated to spectral differences described above, was found by Trudolyubov (2001). During radio-quiet plateaux, the total root mean square (rms) of the QPO is the same as during radio-loud plateaux, but the properties of the noise component are different. Its total fractional rms variability is higher, and an additional broad component around 60–80 Hz is present (see Figure 14, left panel). Indeed, there seem to be two separate “flavors” of C-state PDS: When the QPO frequency is at a certain value, its width and integrated rms are always the same, but the noise level can be significantly different (see also Figure 14, right panel). The association with radio flux differences found by Trudolyubov (2001) is the first direct connection between X-ray noise variability and radio properties. The energy spectrum of the oscillations is hard, with fractional rms increasing with energy, but data from the *RXTE* HEXTE showed a significant turnoff at high energies (30–40 keV; Tomsick & Kaaret 2001). Its first harmonic shows a decrease at 10 keV (Rodriguez et al. 2002a). The LFQPO shows significant and complex phase lags. Reig et al. (2000) found that both QPO and continuum noise show hard lags when the QPO frequency is below 2 Hz, evolving smoothly to soft lags when the QPO frequency exceeds 2 Hz (Figure 15; see also Lin et al. 2000). When the fundamental frequency shows negative (soft) lags, the first harmonic shows positive (hard) lags (Tomsick & Kaaret 2001).

Little work has been done on the timing properties of states A and B. Power spectra were shown by Chen et al. (1997), Markwardt et al. (1999), and Belloni (1999a). As mentioned above, the PDS of the soft states are complex and lack clear narrow QPO peaks like those from state C. A set of PDS from variability classes ϕ , ν , and δ (see Figure 7) have been presented by Ji et al. (2003). These authors also performed a coherence analysis and found that the coherence deviates from unity above a characteristic frequency. A few PDS are also presented by Reig et al. (2003), selected to separate state A and state B.

High-Frequency Quasi-Periodic Oscillations From a set of 31 early *RXTE*/PCA observations of GRS 1915+105, Morgan et al. (1997) discovered the first QPO at frequencies > 50 Hz in a BHC. In only two observations of those analyzed, a significant peak at a frequency of 67.7 and 65.5 Hz was detected, with a width of ~ 4 Hz and a fractional rms variability of 1.1 and 1.6%, respectively.

Its rms increased with energy up to 6% above 12 keV. Hints of the presence of the same oscillation were present in four more observations. Belloni et al. (2001) analyzed the observation when the QPO was strongest (May 5, 1996) and found strong variations in its energy dependence as a function of the much slower B \leftrightarrow A oscillation. In a second observation, they found a broad 27 Hz QPO only during the A intervals. The phase lags of the 65 Hz QPO were studied by Cui (1999), who found hard lags increasing with energy up to 2.3 radians between the 5.2–7.0 keV and the >13 keV bands.

Strohmayer (2001) analyzed 97 PCA observations from 1997 and found in 5 of them a QPO at a frequency (\sim 69 Hz) higher than that found by Morgan et al. (1997). In addition, a second QPO peak at \sim 40 Hz was found in the high-energy data, simultaneous with the 69 Hz peak (see Figure 16).

These oscillations were found in observations of classes γ and ϕ and are therefore associated with states B and A, but not with state C, when the low-frequency QPOs are observed. It is interesting that the three frequencies presented above, 27, 40, and 69 Hz, are roughly in 2:3:5 ratio (see Abramowicz et al. 2003).

A representative set of PDS from the three different states is shown in Figure 17 (from Reig et al. 2003).

2.3 Radio and Infrared Emission

2.3.1 Radio

GRS 1915+105 has turned out to be one of the most spectacular radio sources within our galaxy, displaying not only—like in X-rays—highly variable and structured light curves but also spatially resolvable steady and transient jets at different times.

Radio variability and relativistic jets Mirabel et al. (1993a) reported the first detection of the radio counterpart of GRS 1915+105 as a relatively weak (2.5–5 mJy) source at 20 cm with the Very Large Array (VLA). Although interesting, there was little hint in this first IAU Circular of the excitement to follow. However, by the end of 1993, Mirabel et al. (1993b) and Rodríguez & Mirabel (1993) reported further VLA observations, indicating a highly variable, sometimes very luminous, and possibly even moving radio source.

Early in 1994, Mirabel et al. (1994) published details of the radio and IR counterpart. They demonstrated that the source probably lies behind more than 30 magnitudes of absorption in the optical band—which has to date precluded any identification of an optical counterpart (but see Boër, Greiner & Motch 1996 for a possible I-band counterpart)—and that the radio counterpart showed variability

that was in some way correlated with the X-ray emission. In March 1994, Gerard, Rodríguez & Mirabel (1994) announced a major radio outburst (flux densities > 1 Jy at 20cm) from the source. It was this outburst that was to change the way we look at jets from X-ray binaries: In a ground-breaking paper, Mirabel & Rodríguez (1994) reported apparent superluminal motions in twin-sided radio knots moving away from the core of GRS 1915+105 (Figure 18, left panel). For the first time, superluminal motions—previously a characteristic unique to jets from supermassive black holes in active galactic nuclei—had been observed in our galaxy. The term microquasar, first applied to the galactic X-ray source 1E 1740.7-2942 owing to its large-scale radio lobes (Mirabel et al. 1992), seemed entirely appropriate for GRS 1915+105. The fact that powerful, significantly relativistic ejections could be observed from a black hole transient that, although different in some ways from other transients was not that different, ushered in a new era in the study of jets from stellar mass compact objects. The nonuniqueness of such highly relativistic jets was dramatically highlighted by the discovery of a superluminal jets from another X-ray transient, GRO J1655-40, within one year (Hjellming & Rupen 1995, Tingay et al. 1995).

Rodríguez et al. (1995) reported five months’ radio monitoring of GRS 1915+105, which demonstrated that the source was undergoing repeated major radio flares. Radio monitoring had also begun at the Green Bank Interferometer (GBI) (Foster et al. 1996) and the Ryle Telescope (RT) (Pooley & Fender 1997). Foster et al. (1996) reported detailed GBI monitoring at 2.3 and 8.3 GHz, which identified two states of bright radio emission: flaring (optically thin spectra, rapid decays) and plateaux (flat-topped periods in the light curve with optically thick radio spectra). We consider the plateaux to be a bright subset of the χ class/C state of GRS 1915+105 (also referred to as χ_{RL} by Naik & Rao 2000 and type II hard states by Trudolyubov 2001). A clear example of a plateau state is presented in Figure 19.

That the flaring periods corresponded to further relativistic ejections was assumed and confirmed by Rodríguez & Mirabel (1999), who also noted small apparent changes in the projection of the jets on the sky. Later the same year Fender et al. (1999) reported observations of a major outburst with the UK Multi-Element Radio Linked Interferometer Network (MERLIN), with five times the angular resolution of the VLA at 5 GHz (Figure 18, right panel). These observations revealed again relativistic ejections, but with considerably higher (by approximately 20%) proper motions than those measured with the VLA. Comparison with GBI and RT radio monitoring, and X-ray monitoring with the *RXTE* ASM, indicated that the multiple relativistic ejections observed by Fender et al. (1999) originated in major flares immediately following a protracted plateau phase. The MERLIN observations further revealed significant and variable (possibly rotating) linear polarization in the ejecta, and hints of curvature in the jet

axis, possibly owing to precession.

The beauty of the observations of two-sided proper motions by Mirabel & Rodríguez (1994) and Fender et al. (1999) is that they allow several clear results to be drawn. A maximum distance, under the assumption of an intrinsically symmetric ejection, can be derived as

$$d_{\max} = \frac{c}{\sqrt{(\mu_{\text{app}}\mu_{\text{rec}})}},$$

where μ_{app} and μ_{rec} are the approaching and receding proper motions, respectively, and c is the speed of light. The proper motions reported by Mirabel & Rodríguez (1994) indicated that GRS 1915+105 lay within our galaxy and was therefore an X-ray binary source. The most recent two-sided proper motions, reported in Fender et al. (1999), constrain $d_{\max} \leq 13.6$ kpc (3σ). The observed proper motions can also be used to place a lower limit on the velocity of the radio-emitting knots, independent of distance:

$$v_{\min} = \frac{\mu_{\text{app}} - \mu_{\text{rec}}}{\mu_{\text{app}} + \mu_{\text{rec}}} c,$$

which, when applied to GRS 1915+105, indicates a minimum velocity of $\sim 0.3c$ on VLA scales and $\sim 0.4c$ on MERLIN/Very Long Baseline Array (VLBA) scales (see below). The discussion of what can be derived from the proper motion measurements is expanded upon in Mirabel & Rodríguez (1999) and Fender (2003).

Mirabel & Rodríguez (1994) also noted that the flux ratio between the approaching and receding components was very close to that expected in the case of true bulk motion:

$$\frac{S_{\text{app}}}{S_{\text{rec}}} = \left(\frac{1 + \beta \cos \theta}{1 - \beta \cos \theta} \right)^{k-\alpha},$$

where $\beta = v/c$ and θ are the intrinsic velocity and angle to the line of sight of the jets, α is the spectral index of their radio emission, and k ranges between 2 (for a steady flow) and 3 (for discrete ejections). The observed flux ratios of 8 ± 1 found by Mirabel & Rodríguez (1994) and 6–10 by Fender et al. (1999) correspond to a value of k in the range 1.3–2.3 and indicate true bulk relativistic motions at some level. This does not rule out an origin for the observed knots in moving shocks but does require that the underlying plasma flow has bulk relativistic motion. In more detailed calculations, Bodo & Ghisellini (1995) concluded that the observed patterns could be shocks but still required a bulk motion of $\geq 0.7c$ (see also Atoyan & Aharonian 1999).

The power in these ejections was also found to be very large—applying the minimum energy conditions of Burbidge (1959), Mirabel & Rodríguez (1994) estimated an energy associated with the March 1994 event of 3×10^{46} erg. Conservatively estimating an injection/acceleration timescale of ≤ 3 days, this corresponds to a jet power during this period of $\geq 10^{41}$ erg s $^{-1}$. Atoyan & Aharonian

(1999) and Fender et al. (1999) estimated lower, but still considerable, jet powers of $\geq 10^{38}$ erg s $^{-1}$. Furthermore, as demonstrated in Fender (2003), the observed proper motions only allow us to place a lower limit on the bulk Lorentz factor Γ of the flow, and therefore on total energy associated with the ejections (the total energy $E_{\text{tot}} \sim (\Gamma - 1)E_{\text{int}}$, where E_{int} corresponds to the above minimum energy values). The true value of the initial bulk Lorentz factor for the relativistic ejections, such as those observed by MERLIN, is likely to lie in the range

$$2 \leq \Gamma_{\text{bulk}} \leq 30,$$

where the lower limit can be derived from observations and the upper limit corresponds to a mean jet power of $\sim 10^{41}$ erg s $^{-1}$ over a 12-h jet formation phase (at ~ 45 times the Eddington limit for a $\sim 15 M_{\odot}$ black hole, this should be reasonable!). Clearly, the power expended on particle acceleration and bulk motion during the jet formation episodes could represent a significant, even dominant, fraction of the total accretion power available.

The nature of the compact self-absorbed emission during plateaux was revealed by Dhawan, Mirabel & Rodríguez (2000) who found in observations with the VLBA that it corresponded to a compact, relatively steady jet. They further reported proper motions on small scales that were consistent with those reported by Fender et al. (1999). The lower values for the proper motions reported in VLA observations (Mirabel & Rodríguez 1994, 1999) may be due to resolution effects or genuine deceleration of the ejecta as they propagate further from the launch point. Further very long baseline interferometry (VLBI) observations with the European VLBI Network (EVN) have confirmed the resolved core during plateau states (Giovannini et al. 2001) and suggested that the plateau jet is of lower velocity than the transient ejections, although the reported details were sparse. The most recent dual-frequency VLBA observations (Fuchs et al. 2003b) reveal a compact jet from the source whose size varies as a function of frequency in a way that appears to be consistent with expectations for a self-absorbed outflow (Figure 20).

Shortly after the major relativistic ejections were reported, several groups realized that these jets might leave their imprint on the ISM, just as the jets of AGN produce bright radio lobes. Levinson & Blandford (1996), Kaiser et al. (2000, 2004), Heinz (2002), and others have discussed the formation of shocks in the ISM by these jets. However, although large-scale jet-powered nebulae are known around some X-ray binaries (see, e.g., Fender 2004 and references therein), searches for large-scale radio structures around GRS 1915+105 have been generally unsuccessful (Chaty et al. 2001, Ostrowski & Fürst 2001). Nevertheless, there are hints of associations with nearby IRAS sources that deserve further investigation (Chaty et al. 2001; Kaiser et al. 2004). Note though that these sources are so far distant that if associated it must have been with outbursts

much earlier than the one that has been ongoing for the past decade (Chaty et al. 2001 and discussion therein).

Radio “oscillations” Another major discovery was made with the RT: Pooley (1995) reported “oscillations” at 15 GHz with an apparent period close to 38 min. Monitoring with both instruments continued apace, and in 1997, Pooley & Fender (1997) reported comprehensive long-term radio monitoring at 15 GHz. The presence of quasi-sinusoidal oscillations (see also Rodríguez & Mirabel 1997), with amplitudes up to 50 mJy and periods in the ranges tens of minutes to hours, was unambiguous. Furthermore, Pooley & Fender (1997) demonstrated that oscillations at 15 GHz led those at 8.3 GHz by approximately 4–5 min. Finally, they showed that there appeared to be some connection between these radio oscillations and X-ray “dips” observed at the same time, with a similar recurrence period, by *RXTE* (Figure 21). This was the first example of the great successes that were to come by combining *RXTE* with simultaneous radio and/or IR observations. Fender et al. (1999) noted that approximately four days of radio oscillations separated two major ejection events resolved with MERLIN. Naik et al. (2001) have also discussed the association of dips in the X-ray light curve with radio flaring.

More recently, Klein-Wolt et al. (2002) have reported a comprehensive study of the relation between radio and X-ray emission in GRS 1915+105 (see below for more details). Fender et al. (2002a) reported a detailed study of the radio oscillations from GRS 1915+105, revealing that the delays between two frequencies are not constant from epoch to epoch. Finally, Fender et al. (2002b) reported the detection of circular polarization associated with relativistic ejections from GRS 1915+105 utilizing simultaneous ATCA and MERLIN observations.

2.3.2 Infrared and Millimeter

Infrared Variability Mirabel et al. (1993b, 1994) first identified the near-IR counterpart of GRS 1915+105 as a variable source in the J (1.2 μm), H (1.6 μm), and K (2.2 μm) bands. Whereas spectroscopy and high-resolution imaging (see below) produced some surprises, a key piece in the disc-jet connection came from high time-resolution IR photometry of the source. Mirabel et al. (1996) reported a brightening and reddening of the source in the near-IR following a major ejection event, which they interpreted as reverberation of the event in circum-binary dust. Chaty et al. (1996) reported more rapid near-IR variability. Motivated by this and the discovery of radio oscillations (see above) (Pooley 1995, Pooley & Fender 1997), Fender et al. (1997) performed relatively high time-resolution K-band photometry of GRS 1915+105 and found the source to be oscillating with a comparable amplitude (when dereddened), period, and shape as radio oscillations

observed earlier the same day. They argued that the IR events, like the radio events, were likely to be synchrotron in origin, thereby increasing at a stroke the minimum power associated with these oscillation events by four to five orders of magnitude. Fender et al. (1997) further suggested that IR synchrotron emission could explain the result of Mirabel et al. (1996) (see above) without requiring dust reverberation. Like the major ejections (see above), these smaller, repeated ejections were clearly a major power output channel.

Follow-up to these observations was intense and rapid. Eikenberry et al. (1998a) reported high time-resolution IR photometry simultaneous with *RXTE* observations, confirming the suspected link between events (Figure 22). Mirabel et al. (1998) observed simultaneously in the radio, IR, and X-ray bands (Figure 23). These observations appeared to reveal a hard X-ray dip followed by an IR flare, followed by a radio flare, thereby revealing a progression of the event to lower frequencies, as expected for models with decreasing optical depth in ejecta. Eikenberry et al. (1998b) reported IR spectroscopy during flare/oscillation events, which revealed that the IR emission lines varied in strength in an approximately linear way with the continuum. The mechanism behind this is not immediately obvious because it was already concluded that the continuum was (mostly) synchrotron emission in origin. Eikenberry et al. (1998b) suggested that the lines were being radiatively pumped by the synchrotron flares. Fender & Pooley (1998) presented further simultaneous radio and IR observations, revealing a comparable IR-radio delay to that reported by Mirabel et al. (1998). Ogley et al. (2000) reported “excess” submillimeter emission from GRS 1915+105, and Fender & Pooley (2000) reported simultaneous IR and millimeter (1.3 mm) observations of GRS 1915+105, revealing large oscillation events taking place at both frequencies near the end of an apparently uninterrupted sequence of over 700 events. Eikenberry et al. (2000) presented evidence for weaker IR flaring from GRS 1915+105 that was associated with soft dip/flaring cycles.

At longer wavelengths, Winkler & Trams (1998) and Fuchs et al. (2003a) report ISO observations of GRS 1915+105. One of the observations of Fuchs et al. (2003a), between 4–18 μm , was during a plateau state and is consistent with a flat-spectrum component, probably synchrotron or free-free emission (see below).

Spectroscopy Castro-Tirado, Geballe & Lund (1996) reported K-band spectroscopy of the source, revealing emission lines of HI, HeI, and HeII. Whereas Castro-Tirado et al. (1996) and Eikenberry et al. (1998b) argued that the emission lines probably arose in an accretion disc in a low-mass X-ray binary, Mirabel et al. (1997) argued that the lines were likely to originate in an Oe- or Be-type massive star and that GRS 1915+105 was therefore a high-mass X-ray binary. The origin of these lines remained controversial until the identification of the binary companion by Greiner et al. (2001a,b) (see below).

Resolved Infrared Jets Sams, Eckart & Sunyaev (1996a) reported the discovery of a near-IR jet in K-band speckle imaging of GRS 1915+105 with the ESO New Technology Telescope (NTT). Repeat observations less than one year later revealed that the jet disappeared (Sams, Eckart & Sunyaev 1996b). Eikenberry & Fazio (1997) also found no evidence for extended IR emission from GRS 1915+105 and, although the results of Sams, Eckart & Sunyaev (1996a) appear convincing, it is odd that the IR extension has never been independently verified.

Identification of the Orbit, Companion, and Mass Function Greiner et al. (2001a) finally managed to identify the binary companion to GRS 1915+105 by observing ^{12}CO and ^{13}CO bandheads in H- and K-band spectroscopy using ESO's Very Large Telescope (VLT). These features clearly identified the binary companion as a K- or M-type giant, confirming that GRS 1915+105 was, in fact, a low-mass X-ray binary. More excitingly, photospheric absorption features such as these opened the possibility to perform radial velocity studies of the system to see if, as expected, it contained a black hole. This is precisely what Greiner, Cuby & McCaughrean (2001b) did: In a comprehensive IR spectroscopic study, they obtained an orbital period of 33.5 days with an associated radial velocity semi-amplitude of $140 \pm 15 \text{ km s}^{-1}$ (Figure 24). The resulting mass function (minimum mass for the accreting object) is $9.5 \pm 3.0 M_{\odot}$, indicating a black hole at the $\sim 2.5\sigma$ level. Assuming a lower-limit on the mass of the binary companion of $1.2 M_{\odot}$ and an orbital inclination corresponding to that derived for the relativistic jets by Mirabel & Rodríguez (1994) of 70 ± 2 degrees, they arrived at a most likely mass for the compact object in GRS 1915+105 of $14 \pm 4 M_{\odot}$, making it a strong candidate for the most massive stellar mass black hole known. Several authors have considered the evolution of the GRS 1915+105 binary system in light of this result (e.g., Belczynski & Bulik 2002; Podsiadlowski, Rappaport & Han 2003 ; see also, e.g., King 2004 for a comparison with ultra-luminous X-ray sources in external galaxies). It is important to realize that the binary plane may not be perpendicular to the jet axis (Maccarone 2002), in which case the mass of the black hole in GRS 1915+105 could be significantly greater (although not much smaller) than the estimate of Greiner, Cuby & McCaughrean (2001b).

2.4 Radio and Infrared Evidence for Disc-Jet Coupling

2.4.1 First Connections from Daily Monitoring

The first obvious connections between the disc (X-rays) and jet (radio initially; later the jet was also appreciated to emit in the near-IR), were identified via daily monitoring of the source in multiple bands.

Foster et al. (1996) and Harmon et al. (1997) first demonstrated the clear association between periods of hard X-ray emission and major radio outbursts in GRS 1915+105. Based on the imaging of superluminal ejections associated with just such an outburst by Mirabel & Rodríguez (1994), it was reasonable to make a connection between these long, hard X-ray phases and major ejections. Foster et al. (1996) noted that the radio emission during the hard X-ray phase was actually rather optically thick and coined the phrase plateau states to describe this combination of hard X-ray emission and strong flat-spectrum radio emission. The association with radio flares and ejections was—as discussed below—probably due to the fact that such plateaux generally reverted to softer X-ray states within 10–30 days, and that this transition was accompanied by a major ejection event (Fender et al. 1999, Klein-Wolt et al. 2002). Figure 19 presents multiwavelength radio and X-ray monitoring of GRS 1915+105 through such a plateau phase.

2.4.2 Coupling between X-ray “Dips” and Synchrotron Oscillations

By 1998 it was already established that periods of “hard dips” in the X-ray light curve of GRS 1915+105 on timescales of minutes to hours were associated with events in the IR and radio bands. Following the initial hints in Pooley & Fender (1997), key observations were reported in Eikenberry et al. (1998a,b) and Mirabel et al. (1998). More recently, Klein-Wolt et al. (2002) have undertaken the most thorough study of the connection between the X-ray variability and radio emission, and they highlight a strong link between hard X-ray states and radio emission, and specifically a one-to-one correspondence between hard X-ray (state C) “dips” and radio oscillation events.

It seems clear that, although the details of the physics may not be well understood, each hard dip in a sequence is associated with a radio—millimeter—IR event, which itself is associated with a powerful outflow. Note that Feroci et al. (1999) have reported the association of a radio “flare” from GRS 1915+105, associated with a dip in the X-ray light curve; with hindsight this event seems more like an oscillation event associated with an isolated state C. The key observational characteristics of these oscillation events are as follows:

- Each event is associated with a state C dip followed by a state A/B phase.
- The rise and decay profiles are very similar over a broad range in frequencies (from the radio through the near-IR). This suggests that the optical depth effects do not strongly influence the profile of the event, and that adiabatic expansion losses (which are frequency-independent) dominate the decay phase.
- The events occur with a delay between different frequencies in the sense

that higher frequency events occur earlier; the delays are not constant to better than a factor of two. These delays suggest optical depth effects.

- The energy associated with the events is large, and it is a significant fraction of the contemporaneous X-ray luminosity.

Whether these synchrotron events correspond to the ejection of discrete blobs (e.g., Mirabel et al. 1998), internal shocks in a more continuous flow (Kaiser, Spruit & Sunyaev 2000) or variations in the jet power in a self-absorbed outflow (Collins, Kaiser & Cox 2003) is currently not clear (but see below). That are powerful events – extracting a sizeable fraction of the available accretion energy (assuming it is Eddington limited) seems indisputable (see, e.g., power estimates in Fender & Pooley 2000).

2.4.3 “Steady” Jets in Prolonged Hard X-ray Plateaux

Foster et al. (1996) discovered that prolonged phases of hard X-ray emission—plateau states—were associated with steady, relatively bright, flat-spectrum radio emission, indicating some (self-)absorption of the synchrotron emission. Dhawan et al. (2000) and Fuchs et al. (2003b) have reported direct imaging of an apparently steady radio jet during this phase (Figure 20). The nature of this steady radio emission has been discussed at length in, e.g., Falcke & Biermann (1996), Muno et al. (2001), Klein-Wolt et al. (2002), and Vadawale et al. (2003). We can now be confident that each plateau episode is associated with such emission, which can naturally be explained in terms of a conical self-absorbed jet (e.g., Blandford & Konigl 1979, Hjellming & Johnston 1988, Falcke & Biermann 1996).

2.4.4 Major Ejections After (and Before?) Plateaux

Although empirically well established, the physical connection between X-ray emission and the most spectacular of the jet-related phenomena—the superluminal jets—has been the hardest to understand. This is perhaps not surprising given that they do not repeat quasi-periodically many times in a row (like the oscillation events), nor are they quasi-steady for many days (like the plateaux).

However, a general characteristic did emerge early on, namely that plateau states are generally followed (and perhaps preceded) by major ejection events (e.g., Foster et al. 1996, Fender et al. 1999, Dhawan et al. 2000, Klein-Wolt et al. 2002) (see Figure 19). Furthermore, it seems rather common that the “post plateau flare” (Klein-Wolt et al. 2002) is followed by several days of X-ray/radio oscillations. Klein-Wolt et al. (2002) also noted that the pre-plateau flares are generally stronger than the post-plateau flares. In the study of Fender

et al. (1999), these oscillations appeared for four days between major relativistic ejection events.

2.4.5 The Overall Picture—Two or Three Types of Jets?

Above, we have outlined the observational characteristics of three types of radio emission associated with jets from GRS 1915+105: oscillations, plateaux, and major flares. That the source can readily switch between these modes is evident from the data presented in Fender et al. (1999) and Klein-Wolt et al. (2002) wherein the source

1. Produces a medium-strength optically thin flare (probable ejection event)
2. Enters a plateau state (steady jet)
3. Produces a major flare (discrete relativistic ejection)
4. Enters several days of oscillations (repeated small ejections)
5. Reflares several times (discrete relativistic ejections)

We have no reason to think that this behavior was particularly unique (inspection of the radio light curves in, e.g., Pooley & Fender 1997 suggest that it definitely is not).

How many types of jet production are required to explain this phenomenology? The answer would seem to be two or three.

The steady plateau jets and the major ejections are clearly different, as outlined in Table 1.

[Table 1 about here.]

It is possible that the oscillation events correspond to a third class of jet formation, but it is likely that they do not. Based on the empirical connections established in Klein-Wolt et al. (2002), we can see that the oscillations are in fact associated with a combination of steady state C phases and with transitions from this state C to a softer state. Note that Naik & Rao (2000) and Naik et al. (2001) interpret sequences of dips/oscillations as the cause of the major flare events, although this seems at odds with observations where many days of oscillations have not been associated with major flaring (e.g., Pooley & Fender 1997, Fender & Pooley 2000).

We therefore conclude—being consistent with Occam’s razor—that the oscillation events are the equivalent of the optically thin events that follow plateaux. We shall see in the next section that this interpretation is supported by drawing analogies with other objects. One obvious consequence of this interpretation is that, regardless of the velocity of the steady plateau jets, the oscillation events should also be associated with relativistic bulk velocities.

3 Other Sources: GRS 1915+105 in Context

3.1 Black Hole X-ray Binary States

Some of the observed X-ray and IR/radio properties of GRS 1915+105 are clearly unique to this system. On the other hand, many other properties are similar to those observed from other black-hole binaries. In this Section, we briefly summarize the general common properties of other systems, leaving out other peculiarities, to compare them with those of GRS 1915+105. We do not discuss the low-luminosity quiescent state because GRS 1915+105 has been very bright since its discovery, not allowing a comparison with quiescent systems.

Even after years of *RXTE* data from both the (few) persistent systems and the (many) transient systems, our general picture of the X-ray properties of BHCs is not much clearer in the sense that there are a number of significant exceptions to the states-scheme discussed below. Also on the theoretical side, there is not much consensus as to the physical origin of some of the observed spectral components, the timing feature, nor the physical parameters driving state transitions. Yet, a classification in terms of source states is very useful and our only current way to provide an observational view for the development of theoretical models.

Currently, we identify three main “canonical” states in BHCs, identified by their timing and spectral properties. We summarize here their basic properties; for a complete description see, e.g., Tanaka & Lewin (1995), McClintock & Remillard (2004), J. Homan & T. Belloni (manuscript in preparation).

3.1.1 The Low/Hard State

In this state, the energy spectrum is dominated by a power-law-like component, with photon index typically ~ 1.6 , showing a clear high-energy cutoff at approximately ~ 100 keV. An additional weak very soft component, probably associated with the thermal disc, might be observable below 1 keV if the interstellar absorption is not too high. This state is positively associated only with the early and final phases of the outburst of transient systems, which indicates its association to relatively lower values of mass accretion rate. In the timing domain, the PDS shows strong ($\sim 30\%$ – 40% fractional rms) variability, consisting of few band-limited components and sometimes a low-frequency QPO, whose characteristic frequencies appear to be correlated with accretion rate.

The low/hard X-ray state (LS) in canonical X-ray binaries is usually, probably ubiquitously, associated with flat-spectrum radio emission, which varies in a correlated way with the X-ray emission (Fender 2001, 2004). Specifically, the radio spectral index $\alpha \geq 0$ (where $\alpha = \Delta \log S_\nu / \Delta \log \nu$, i.e., $S_\nu \propto \nu^\alpha$). The radio luminosity varies with the soft X-ray luminosity approximately as $L_{\text{radio}} \propto L_X^{0.7}$

(Corbel et al. 2003, Gallo et al. 2003) until the transition to softer states, when it drops dramatically (Fender et al. 1999, Corbel et al. 2001, Gallo et al. 2003). In the bright hard state system Cygnus X-1, this radio emission has been resolved into a steady milliarsecond-scale jet (Stirling et al. 2001).

3.1.2 The High/Soft State

Here the energy spectrum is dominated by a thermal component, usually modeled as a disc-blackbody with an inner temperature of 1–2 keV. A much weaker power-law component is present, with a steep photon index. No apparent high-energy cutoff is observed in high signal-to-noise spectra. Very little variability is observed, with the PDS showing a power-law component with a few percent fractional rms. This state is usually found in the central parts of outbursts of transients, indicating its association to a higher mass accretion rate than the LS.

The high/soft state (HS) is associated with a dramatic drop in the radio emission compared to that observed in the LS, essentially to undetectable levels (Fender et al. 1999, Gallo et al. 2003), representing a drop in radio luminosity by at least a factor of 30. Sometimes optically thin radio emission is associated with the HS, and is probably associated with shocks in material distant from the binary core, which is itself no longer a radio source (e.g., Gallo et al. 2004).

3.1.3 The Intermediate/Very High State

The name of this state indicates its dual nature and the complex history behind it. The energy spectrum is characterized by intermediate properties between the LS and the HS, with both a strong thermal component and a power-law component with $\Gamma \sim 2.5$. The relative contribution of these two components to the 1–10 keV flux can vary between 10% and 90%. As in the HS case, no high-frequency cutoff has been measured in the hard component (Grove et al. 1998). The PDS is either a band-limited noise with a strong low-frequency QPO or a weaker steep power-law component, sometimes with a strong and narrow QPO at a frequency of ~ 6 Hz (see Nespoli et al. 2003; P. Casella, T. Belloni, J. Homan & L. Stella, submitted manuscript; J. Homan & T. Belloni, manuscript in preparation). This is the state when high-frequency QPOs have been observed in a few systems. From the analysis of the outburst of a number of transients, it is emerging that the appearance of this state is both related and unrelated to the variation of mass accretion rate. The transition between LS and HS and the reverse transitions, happening at very different accretion rates, take place through a period of intermediate/very high state (VHS/IS). On the other hand, clear, brief instances of VHS/IS are observed during the HS periods, indicating

that another parameter different from \dot{M} can trigger a transition. Notice that in many systems, for instance, XTE J1550-564 (Cui et al. 1999) and GX 339-4 (Belloni et al. 2002), the PDS of the LS at the beginning of the outburst evolve in a smooth manner, with all characteristic frequencies increasing in time, and this smooth evolution continues into the VHS/IS, despite the fact that the spectral properties change considerably.

The association of radio emission with the VHS/IS is unclear. Corbel et al. (2001) demonstrated that when the X-ray binary XTE J1550-564 entered a relatively soft IS, the radio emission dropped in a way reminiscent of the radio quenching in the HS. Furthermore, the radio quenching in Cyg X-1 (Gallo et al. 2003) may also be associated with a transition to the IS and not the true HS. On the other hand, many transient outbursts are associated with a rapid rise to the VHS, and such outbursts are nearly always associated with bright optically thin events (Fender & Kuulkers 2001).

3.2 GRS 1915+105 A/B/C States and Other Systems

Three states are found in GRS 1915+105 and three main states are known in other BHCs. It is natural to compare them to see if they are similar or perhaps even the same states under different names, although the timescales of transitions are obviously much different. A comparison based mainly on timing properties was done by Belloni (1999b) and Reig et al. (2003). Table 2 shows the six states in terms of X-ray spectral and timing properties, with a comment on the jet properties. Spectrally, it is clear that the maximum inner temperature of the disc component is higher in GRS 1915+105, related to the high value of the accretion rate. However, the disc component behaves generally in a similar way during the state C and the LS. Indeed, there is the suggestion that the inner radius disk during the LS of BHCs is larger than in the other states (see, e.g., Esin et al. 1997), although the physical model associated to this might be different. Because the timing properties of LS and VHS/IS seem to be linked (see above), it is therefore possible that the hardest intervals of GRS 1915+105 are instances of a LS, and indeed the power-law index does reach LS-like values. However, the absence of a high-energy cutoff measured by *CGRO*/OSSE would argue against this interpretation (Zdziarski et al. 2001). In Table 2 we put a question mark in the corresponding box, as *RXTE* measurements shown before seem to indicate the actual presence of a high-energy cutoff that can reach values as low as a few dozen keV. Both states A and B have variability properties that would associate both of them to the VHS in its steep version (see above).

The overall pattern of behavior of the jets in GRS 1915+105 also seems to be qualitatively very similar to more “normal” black hole X-ray binaries. That is,

it follows the basic rules of hard states associated with radio emission/jet production, soft states associated with a quenching of the radio emission/cessation of jet production, and (rapid) transitions between hard and soft states associated with bright optically thin events. The direct imaging of the steady jets in plateau states seems to be directly comparable to the imaging of such jets (albeit much weaker) from Cyg X-1 in the LS. Finally, the superluminal ejection events are likely to be the same phenomenon as has been directly imaged during bright transient outbursts for some other systems (most notably GRO J1655-40, but see references in Fender & Kuulkers 2001).

Our conclusion is that probably all three states of GRS 1915+105 are instances of something similar to the VHS/IS observed in other systems, associated to the high accretion rate value for this source, although during the hardest intervals a LS might be reached.

[Table 2 about here.]

3.3 Active Galactic Nuclei

We have discussed the disc-jet coupling in GRS 1915+105 and compared it with other accreting stellar-mass black holes in X-ray binary systems. But what about the connection to supermassive black holes (SMBH) in AGN? One of the great potentials of X-Ray Binary (XRB) research has been the possibility that the physics can be scaled up in size and timescale to AGN, and thereby provide us with insights into the workings of the most powerful engines in the universe. The discovery of the large power and broad ubiquity of jets from BHC XRBs has only heightened this interest. With a general assumption that physical timescales scale with the mass of the black hole (e.g., Sams, Eckart & Sunyaev 1996a and references therein), even one hour of disc-jet coupling in a $10 M_{\odot}$ black hole probes an equivalent timescale of ~ 1000 years in a $10^8 M_{\odot}$ SMBH.

GRS 1915+105 displays a steady jet during plateau states. The X-ray and radio luminosities during this state are compatible with the universal relation found for the LS of X-ray binaries, namely $L_{\text{radio}} \propto L_X^{0.7}$ (Gallo et al. 2003). Merloni et al. (2003) and Falcke et al. (2003) have, with the inclusion of a mass term, found that a closely related expression can fit the $L_{\text{radio}}:L_X:M_{\text{BH}}$ plane for X-ray binaries (including GRS 1915+105) and AGN (note that Falcke et al. 2003 restrict themselves to low luminosity AGN). Therefore, the steady jet in the plateau states is directly comparable with those in AGN not only qualitatively but quantitatively (see also earlier discussion in Falcke & Biermann 1996). Furthermore, Maccarone et al. (2003) present evidence for quenching of the radio emission in AGN in the same range of Eddington-fraction X-ray luminosities (approximately 2%–10% Eddington) as observed in the soft states

of X-ray binaries (Figure 25).

The timescales associated with, for example, state transitions and transient jet formation can vary widely (by factors of at least 10^4) for black holes of (probably) very similar masses, so its not obvious how to scale up to SMBH, at least until the coupling with other parameters, most likely accretion rate, is understood. Nevertheless, Marscher et al. (2002) have claimed to see an equivalent of the hard dip–radio flare cycle, made famous by GRS 1915+105, in the AGN 3C 120 (Figure 26, see color insert). They find dips in the X-ray lightcurve, with a frequency of $\sim 1/\text{year}$, with corresponding hardening of the X-ray spectrum. They further connect these dips to superluminal ejection events directly imaged with VLBI. The ratio of masses $10^5 \leq M_{3C120}/M_{\text{GRS1915+105}} \leq 10^6$ means that events of timescales ~ 1 year in 3C 120 would correspond to timescales of seconds or minutes in GRS 1915+105, close to those observed. Note that the observation of these dips being associated with highly relativistic ejections is consistent with the conclusion drawn earlier that the oscillation events are probably associated with large bulk velocities.

We can therefore conclude that the physics of disc-jet coupling in XRBs and AGN are very closely linked, and that by studying the nearby XRBs—and GRS 1915+105 in particular—we may understand the flow of energy to and away from SMBH at the centers of galaxies over timescales of millions, or even billions, of years.

4 Interpretation: Many Flavors of Disc-Jet Coupling or Just One?

On the basis of our detailed studies of GRS 1915+105, we can make some progress with our understanding of the coupled accretion:outflow progress in accreting black hole systems.

4.1 Hard States and Jet Formation

As discussed above, protracted spells in hard X-ray states are associated with steady jet formation and long periods in soft states are not. Such observations, also in the context of similar behavior in other X-ray binaries (Fender 2004 and references therein) have been considered as strong evidence for the association of magnetohydrodynamic (MHD) outflows with large scale-height accretion flows (e.g., Meier 2001, Meier et al. 2001). The hard X-ray component in such states is generally supposed to arise in some form of Comptonization (e.g., Sunyaev & Titarchuk 1980, McClintock & Remillard 2004), in which case a clear connection

between the “base” of the outflow and this Comptonizing corona is required (see discussions in Munro et al. 2001, Zdziarski et al. 2003, Fender 2004). Alternatively, the hard X-ray emission may arise directly in the jet via Comptonization (see discussion in Atoyan & Aharonian 1999) or, more radically, optically thin synchrotron emission (Markoff et al. 2001, Vadawale et al. 2001). In either case, a clear coupling between the hot plasma responsible for the hard X-ray emission, including its associated strong X-ray variability, and the production of a jet requires explanation in future models. However, this is only part of the story.

4.2 On the Trigger of Optically Thin Events

Empirically, we can also suggest that hard-to-soft state transitions are associated with resolvable ejection events, but is there a unique signature in the X-ray emission that tells us precisely when this event occurs?

Mirabel et al. (1998) suggested that the brief spike seen toward the end of the state-C dip during the oscillations of GRS 1915+105 corresponded to the “launch” of the radio oscillation event. During this spike, the X-ray spectrum softened dramatically, indicating a rapid change in the state of the accretion flow. However, an overriding problem with seeing clearly the disc-jet coupling in GRS 1915+105 (despite the many advantages the source offers) has been that the rise, decay, and recurrence times of the synchrotron events are all comparable. In general, a synchrotron event begins to rise before the previous event is fully decayed, so observing the beginning of the “flare” phase is difficult.

By drawing analogies with other X-ray binaries whose temporal evolution is a little more subdued, we can learn more. Fender, Belloni & Gallo (2004b) have studied in detail the light curves of GRS 1915+105 and three other black hole transients—GX 339-4, XTE J1859+226, and XTE J1550-564—to determine at what point the optically thin radio flare occurred with respect to the X-ray state. The results indicate that the radio event occurs during a local peak in the X-ray light curve, which corresponds to the end of a phase of softening in the X-ray spectrum. In terms of GRS 1915+105, the source makes a transition from state C to states A/B. In terms of the canonical states of other X-ray binaries, such as those listed above, the X-ray peak corresponds to neither the canonical LS or the canonical HS, but to a transition from a “soft” VHS/IS to a “hard” VHS/IS (often en route between the LS and HS).

In many, possibly most, of the more conventional transients, the spectral evolution of the source around the time of the ejection can be tracked more clearly than in GRS 1915+105. What is generally observed is a peak in the LS (e.g., Brocksopp et al. 2002, Maccarone & Coppi 2003, Yu et al. 2003). At this point the strongest self-absorbed jet is probably being produced. Subsequently, most

sources transit to a softer X-ray peak, which corresponds to the VHS/IS, and then later to the canonical HS. It is at the VHS/IS peak that the optically thin radio event occurs; subsequently, the jet is "off" until the return to a harder X-ray state. Applying the knowledge we have gained from these other transients to GRS 1915+105, we assert that the optically thin ejection event occurs at the state C \rightarrow state A transition.

4.3 Jet Power and Velocity

The power associated with the strongest steady jets (those around the LS peak in the X-ray light curve) and the subsequent optically thin events seems to be remarkably close. We can demonstrate this in the following. Fender, Gallo & Jonker (2003) have presented a simple formula for estimating the power in a jet in the LS of an X-ray binary:

$$L_J = AL_X^{0.5},$$

where L_J and L_X are the powers in Eddington units in the jet/outflow and radiation from the accretion flow (primarily X-rays), respectively. The value of the constant is estimated as $A \geq 6 \times 10^{-3}$. Note that Malzac, Merloni & Fabian (2004) have suggested that all low-state sources are jet-dominated, in which the value of the normalization is much larger: $A \geq 0.1$.

Fender, Belloni & Gallo (2004b) have further compiled estimates of the power associated with optically thin ejection events as a function of the corresponding peak (VHS/IS) X-ray luminosity and found a function of the form

$$L_{\text{jet}} = BL_X^{0.4 \pm 0.1},$$

where the exponent (0.4 ± 0.1) results from a fit to multiple independent estimates. These power estimates are made assuming equipartition on the basis of observations of rise times and luminosities of radio events (see Fender et al. 2004b for more details). This is in contrast to the estimates for the steady jets, which are based on broadband spectra and estimates of radiative efficiency (Fender et al. 2003 and references therein) or models for the production of correlated optical and X-ray variability (Malzac et al. 2004).

The normalization for the transients jets, $B \sim 0.5$ (with a large uncertainty, probably as much as an order of magnitude larger or smaller), is directly comparable to the normalization A estimated for the steady jets above (assuming no significant advection of accretion energy in either case). Given the completely independent methods used to estimate the jet power in the two regimes, it is remarkable that the exponents of the two functions are the same within uncertainties. In the event that the estimate for A of Malzac et al. (2004) is closer to

reality than the lower limit given in Fender et al. (2003), then the normalizations are also very close. From this we draw the conclusion that the power associated with the strongest self-absorbed jet, and that associated with the subsequent optically thin flare, are comparable (within an order of magnitude or so). This strongly suggests a rather smooth function in the relation between jet power and X-ray luminosity, and not two completely independent mechanisms for powering the two types of jet.

As noted in Gallo et al. (2003), and hinted at for GRS 1915+105 (see above), it seems that the velocity of the steady jets is also lower than that associated with the optically thin ejection events. This is based on the fact that the spread around a common $L_{\text{jet}} \propto L_X^{0.7}$ relation for all black hole XRBs in the LS requires $v_{\text{LS}} \leq 0.8c$ (for a random distribution of viewing angles), otherwise Doppler boosting would result in a larger scatter. Fender et al. (2004b) have refined this fit and compiled multiple pieces of evidence that the Lorentz factor associated with the optically thin ejections of transient XRBs is $\Gamma \geq 2$. Therefore, although we do not know the form of the function (e.g., it could be step-like or continuous), it seems clear that the transient jets have larger bulk Lorentz factors than the steady jets.

4.4 A Unified (Toy) Model of Disc-Jet Coupling

In the following, we attempt to construct a semi-quantitative model for the radio emission in GRS 1915+105 that is hopefully relevant to other X-ray binaries and to AGN. In order to lay the foundations for this model, we summarize some of the key physical indicators:

- Prolonged “hard” X-ray states (e.g., canonical LS, GRS 1915+105 state C) are associated with steady production of self-absorbed jets.
- Prolonged “soft” X-ray states (e.g., canonical HS, GRS 1915+105 states A and B) are associated with a suppression of jet production.
- During the transition between hard and soft X-ray states, an optically thin ejection event occurs. In the canonical definitions of states, this event occurs at the VHS/IS peak, close to the end of a phase of X-ray spectral softening. This corresponds to a transition from state C to state A in GRS 1915+105 (the C to B channel is not observed; see Figure 8).
- The transient jets associated with these events have significantly larger bulk Lorentz factors than those associated with the steady jets.

Based on these observational results, we have arrived at the following semi-quantitative picture of the evolution of the disc-jet coupling during X-ray binary

outbursts in general, and those of GRS 1915+105 in particular. The picture is summarized in Figure 27 (see color insert), and in the text below.

The upper panel in Figure 27 is a hardness-intensity diagram for the X-ray emission from a given source. The canonical LS and HS correspond to nearly vertical strips at the extreme right (hard) and left (soft) of the panel, respectively. Practically the entire range in hardness between these two canonical states represents VHS/IS of varying hardness. We suggest that above a certain hardness (phases i and ii) a jet is produced whose strength correlates with that of the X-rays in the nonlinear way found by Corbel et al. (2003) and Gallo, Fender & Pooley (2003). Below that hardness (phase iv) a jet is not produced; these two regimes correspond to the regions right and left of the vertical line in Figure 27, respectively. We propose that as a source spectrum softens and it approaches the line from the right, the velocity of the jet increases monotonically. At first, this increase is insignificant for the energetics of the outflow, which is not highly relativistic (bulk Lorentz factor $\Gamma \sim 1$). However, around the time that the source crosses the line (phase iii), which generally corresponds to a peak in the soft X-ray flux, the jet velocity increases very rapidly ($\Gamma \geq 2$) before the jet is shut off. Such a rapid increase in jet velocity would produce a shock in the preexisting, slower-moving, jet, which would manifest itself in an optically thin flare with large bulk motions.

For most X-ray binaries, an outburst follows a path similar to that indicated by the solid arrows in Figure 27. The “quiescent” state of such sources can be found by extending the LS branch vertically downward. Often, sources will exhibit a few secondary flaring states in the same outburst, associated with further optically thin radio flares (e.g., GRO J1655-40, XTE J1550-564, XTE J1859+226—see, e.g., Brocksopp et al. 2001, Homan et al. 2001), but these are usually of declining strength. It is interesting to note that in the model of Vadawale et al. (2003), this declining sequence may be naturally explained by the first event having considerably more material in front of it with which to interact (because there was a long phase of steady jet production in the “quiescent” state and LS). In any case, GRS 1915+105 seems to remain, for most of the time, very close to the dividing line between jet-producing states and states without jets. The radio–mm–IR–X-ray “oscillation” events (e.g., Figures 3, 13, 21, and 23) for which GRS 1915+105 is so famous may be compared to the encircled region in the upper-left of the diagram, with the direction of a typical oscillation being indicated by the dashed arrow. In this picture, GRS 1915+105 is repeatedly entering the jet-producing state then crossing the dividing line to jet-free states. Each transition from right to left is associated with an optically thin event; those from left to right are not. Sometimes GRS 1915+105 remains in the hard state (state C) for considerably longer and may extend across the upper branch toward the canonical LS. However, the transition from this state inevitably involves crossing the line

from right to left once more, producing a major flare event.

This model should be considered as a synthesis of previous observational results and theoretical interpretations (although any errors resulting from the synthesis are entirely ours!). Mirabel et al. (1998) first suggested the idea that the X-ray “spike” at the end of hard “dips” might correspond to the moment of jet production. We have expanded on this to show that in other X-ray binaries it is the (secondary) VHS/IS peak and not the (initial) LS peak that corresponds to the optically thin radio flare. Meier (1999) discussed a dramatically (discontinuously) varying jet speed in response to varying conditions in the accretion flow. The internal-shock model based on varying flow speeds in a semicontinuous jet was originally developed for the jets of the AGN M87 (Rees 1978), and later considered for gamma-ray bursts (Rees & Meszaros 1994) and generically for radio-loud quasars (Spada et al. 2001). Kaiser et al. (2000) considered internal shock models for GRS 1915+105 and Vadawale et al. (2003) explicitly considered “post-plateau flares” as resulting from shocks generated by fast moving ejecta interacting with a slower-moving outflow produced during the plateau. Estimates of the jet power in steady and transient phases are more recent (Corbel et al. 2003; Gallo et al. 2003; Fender et al. 2003, 2004b), as is the certainty that the transient jets are considerably more relativistic than the steady jets (Gallo et al. 2003, Fender et al. 2004b).

The model as it stands is mainly phenomenological, but there are some clues to the underlying physics. For example, the jet velocity seems to increase as the optically thin accretion disc moves ever closer to the central accreting object, only becoming significantly relativistic in the very final stages. This may naturally reflect the escape velocity of matter from the inner edge of the accretion disc, which will remain almost constant until it enters regions of significant spacetime curvature within a few gravitational radii of the black hole (but see Fender et al. 2004a, where a highly relativistic jet from a neutron star is in contradiction with the “escape velocity” scenario). This is consistent with the evolution of the X-ray colors, but what exactly happens at this point? It could be that the soft state, for some reason (e.g., no significant vertical magnetic field or extreme Compton cooling of relativistic electrons), inhibits jet formation, and that the optically thin flare was a last gasp from the jet before it is suppressed. On the other hand, it may be that the sudden increase in jet velocity/power is enough to force the accretion flow to settle into a different state, in which case the state change is a result of, not a cause of, the radio ejection event. The similarity of the formulae for the power associated with the two types of jet may argue for a common underlying mechanism, which is simply the release of gravitational potential in the accretion flow. Alternatively, the boost in the jet velocity, and possibly power, for the very smallest disc radii may be in response to a sudden additional contribution from the black hole spin.

Finally, what makes GRS 1915+105 so special? As noted above, the evolution of outbursts from other X-ray transients typically follow the path of the solid lines in Figure 27. Although some (see, e.g., Homan et al. 2001, Brocksopp et al. 2002) may make a small number of repeated phase iii transitions, resulting in several ejection events, they have all returned to relative obscurity within a year or so. GRS 1915+105 has, on the contrary, been very luminous and active for ≥ 10 years. It seems clear that its unusual behavior is a result of a very high (at times probably super-Eddington) accretion rate being maintained for a very long time, probably as a consequence of binary evolution (the orbital period of GRS 1915+105 is exceptionally long for an X-ray transient). In this sense, it is comparable to the brightest Quasars among the sample of AGN.

5 Conclusions

In this review, we discuss at length the observational properties of GRS 1915+105 in the X-ray, IR, and radio bands one decade after the discovery of highly relativistic jets from the source, the first in our Galaxy. A connection between the X-rays and the longer-wavelength (IR and radio) emission in this source is unambiguous, and as a result it has become one of the key systems for our understanding of the disc-jet coupling. Placing the system into context, we have argued that its properties are not that dissimilar from the X-ray states observed in other black hole binaries. Beyond this, the relation of disc-jet coupling in X-ray binaries to that in AGN is now finally on a quantitative footing, and we can be confident that insights drawn from GRS 1915+105 will be relevant for the disc-jet connection around black holes of all masses. Consequently we have proposed a toy model for the disc-jet coupling in GRS 1915+105—heavily inspired by other, earlier works—that requires a minimum (i.e., one) different mode of jet formation and, we hope, is consistent with the picture for other black hole systems.

Acknowledgements

The authors thank Sergio Campana, Elena Gallo, Marc Klein-Wolt, Thomas Maccarone, and Simone Migliari for many useful comments on earlier drafts of this review.

References

Abramowicz MA, Karas V, Kluzniak W, Lee WH, Rebusco P. 2003. *Publ. ASJ* 55:467–71

- Alexandrovich N, Borozdin K, Sunyaev R. 1994. *IAU Circ. No. 6080*
- Atoyan AM, Aharonian FA. 1999. *MNRAS* 302:253–76
- Belczynski K, Bulik T. 2002. *Ap. J.* 574:L147–50
- Belloni T. 1999a. *Astrophys. Lett. Comm.* 38:225–28
- Belloni T. 1999b. *MPE Rep.* 272:82–85
- Belloni T. 2001. In *The Neutron Star—Black Hole Connection, NATO ASI, Elounda*, C567:295–300. Dordrecht: Kluwer
- Belloni T, Klein-Wolt M, Méndez M, van der Klis M, van Paradijs J. 2000. *Astron. Astrophys.* 355:271–90
- Belloni T, Méndez M, King AR, van der Klis M, van Paradijs J. 1997a. *Ap. J. Lett.* 479:145–48
- Belloni T, Méndez M, King AR, van der Klis M, van Paradijs J. 1997b. *Ap. J. Lett.* 488:109–12
- Belloni T, Méndez M, Sánchez-Fernández C. 2001. *Astron. Astrophys.* 372:551–56
- Belloni T, Nespoli E, Homan J, van der Klis M, Lewin WHG, et al. 2002. *New Views on Microquasars*, pp. 83–85. Kolkata, India: Cent. Space Phys.
- Blandford RD, Königl A. 1979. *Ap. J.* 232:34–48
- Bodo G, Ghisellini G. 1995. *Ap. J.* 441:L69–71
- Boër M, Greiner J, Motch C. 1996. *Astron. Astrophys.* 305:835–38
- Brocksopp C, Fender RP, McCollough M, Pooley GG, Rupen MP, et al. 2002. *MNRAS* 331:765–75
- Burbidge GR. 1959. *Ap. J.* 12
- Castro-Tirado AJ, Brandt S, Lund N. 1992. *IAU Circ. No. 5590*
- Castro-Tirado AJ, Brandt S, Lund N, Laphsov I, Sunyaev RA, et al. 1994. *Ap. J. Suppl.* 92:469–72
- Castro-Tirado AJ, Davies J, Brandt S, Lund N. 1993. *IAU Circ. No. 5830*
- Castro-Tirado AJ, Geballe TR, Lund N. 1996. *ApJ* 461:L99–101
- Chaty S, Mirabel IF, Duc PA, Wink JE, Rodríguez LF. 1996. *Astron. Astrophys.* 310:825–30
- Chaty S, Rodríguez LF, Mirabel IF, Geballe TR, Fuchs Y, et al. 2001. *Astron. Astrophys.* 366:1035–46
- Chen X, Swank JH, Taam RE. 1997. *Ap. J. Lett.* 477:41–44
- Collins RS, Kaise CR, Cox SJ. 2003. *MNRAS* 338:1365–87
- Corbel S, Kaaret P, Jain RK, Bailyn CD, Fender RP, et al. 2001. *Ap. J.* 554:43–48
- Corbel S, Nowak MA, Fender RP, Tzioumis AK, Markoff S. 2003. *Astron. Astrophys.* 400:1007–12
- Cui W, Zhang SN, Chen W, Morgan EH. 1999. *Ap. J. Lett.* 512:43–46
- Dhawan V, Mirabel IF, Rodríguez LF. *Ap. J.* 543:373–85
- Eikenberry SS, Fazio GG. 1997. *Ap. J.* 476:281–90
- Eikenberry SS, Matthews K, Morgan EH, Remillard RA, Nelson RW. 1998a. *Ap. J.* 494:L61–64

- Eikenberry SS, Matthews K, Muno M, Blanco PR, Morgan EH, Remillard RA. 2000. *Ap. J.* 532:L33–36
- Eikenberry SS, Matthews K, Murphy TW Jr, Nelson RW, Morgan EH, et al. 1998b. *Ap. J.* 506:L31–34
- Esin AA, McClintock JE, Narayan R. 1997. *Ap. J.* 489:865–89
- Falcke H, Biermann PL. 1996. *Astron. Astrophys.* 308:321–29
- Falcke H, Koerding E, Markoff S. 2003. *Astron. Astrophys.* In press (astro-ph/0305335)
- Fender RP. 2001. *MNRAS* 322:31–42
- Fender RP. 2003. *MNRAS* 340:1353–58
- Fender RP. 2004. In *Compact Stellar X-ray Sources*. Cambridge, UK: Cambridge Univ. Press. In press (astro-ph/0303339)
- Fender RP, Belloni TM, Gallo E. 2004b. *MNRAS* Submitted
- Fender RP, Gallo E, Jonker PG. 2003. *MNRAS* 343:L99–103
- Fender RP, Garrington ST, McKay DJ, Muxlow TWB, Pooley GG, et al. 1999. *MNRAS* 304:865–76
- Fender RP, Hjellming RM, Tilanus RPJ, Pooley GG, Deane JR, et al. 2001. *MNRAS* 322:L23–27
- Fender RP, Kuulkers E. 2001. *MNRAS* 324:923–30
- Fender RP, Pooley GG. 1998. *MNRAS* 300:573–76
- Fender RP, Pooley GG. 2000. *MNRAS* 318:L1–5
- Fender RP, Pooley GG, Brocksopp C, Newell SJ. 1997. *MNRAS* 290:L65–69
- Fender RP, Rayner D, Trushkin SA, O’Brien K, Sault RJ, et al. 2002a. *MNRAS* 330:212–18
- Fender RP, Rayner D, McCormick DG, Muxlow TMB, Pooley GG, et al. 2002b. *MNRAS* 336:39–46
- Fender RP, Wu K, Johnston H, Tzioumis T, Jonker P, et al. 2004a. *Nature* 427:222–24
- Feroci M, Matt G, Pooley G, Costa E, Tavani M, Belloni T. 1999. *Astron. Astrophys.* 351:985–92
- Foster RS, Waltman EB, Tavani M, Harmon BA, Zhang SN, et al. 1996. *ApJ* 467:L81–84
- Fuchs Y, Mirabel IF, Claret A. 2003a. *Astron. Astrophys.* 404:1011–21
- Fuchs Y, Rodríguez J, Mirabel IF, Chaty S, Ribó M, et al. 2003b. *Astron. Astrophys.* 409:L35–39
- Gallo E, Corbel S, Fender RP, Maccarone TJ, Tzioumis AK. 2004. *MNRAS* 347:L52
- Gallo E, Fender R, Pooley G. 2003. *MNRAS* 344:60–72
- Gerard E, Rodríguez LF, Mirabel IF. 1994. *IAU Circ. No.* 5958
- Giovannini G, Feretti L, Tordi M, Venturi T, Massaglia S, et al. 2001. *Astrophys. Space Sci. Suppl.* 276:111–12

- Greenhough J, Chapman SC, Chaty S, Dendy RO, Rowlands G. 2003. *MNRAS* 340:851–55
- Greiner J. 1993. *IAU Circ. No. 5786*
- Greiner J, Cuby JG, McCaughrean MJ, Castro-Tirado AJ, Mennickent RE. 2001a. *Astron. Astrophys.* 373:L37–40
- Greiner J, Cuby JG, McCaughrean MJ. 2001b. *Nature* 414:522–524
- Greiner J, Morgan EH, Remillard RA. 1996. *Ap. J. Lett.* 473:107–10
- Grove JE, Johnson WN, Kroeger RA, McNaron-Brown K, Skibo JG, Philips BF. 1998. *Ap. J.* 500:899–908
- Hannikainen DC, Vilhu O, Rodriguez J, Brandt S, Westergaard NJ, et al. 2003. *Astron. Astrophys.* 411:L451
- Harmon BA, Paciesas WS, Fishman GJ. 1992. *IAU Circ. No. 5619*
- Harmon BA, Deal KJ, Paciesas WS, Zhang SN, Robinson CR, et al. 1997. *Ap. J. Lett.* 477:85–89
- Heinz S. 2002. *Astron. Astrophys.* 388:L40–43
- Hjellming RM, Han H. 1995. In *X-ray Binaries*, p. 308. Cambridge, UK: Cambridge Univ. Press
- Hjellming RM, Johnston KJ. 1988. *Ap. J.* 328:600–9
- Hjellming RM, Rupen MP. 1995. *Nature* 375:464–68
- Homan J, Wijnands R, van der Klis M, Belloni T, van Paradijs J, et al. 2001. *Ap. J. Suppl. Ser.* 132:377–402
- Jahoda K, Swank JH, Giles AB, Stark MJ, Strohmayer T, et al. 1996. *Proc. SPIE* 2808:59–70
- Janiuk A, Czerny B, Siemiginowska A. 2000a. *Ap. J. Lett.* 542:33–36
- Janiuk A, Czerny B, Siemiginowska A. 2000b. *Ap. J.* 576:908–22
- Ji JF, Zhang SN, Qu JL, Li TP. 2003. *Ap. J. Lett.* 584:23–26
- Jorstad SG, Marscher AP, Mattox JR, Wehrle AE, Bloom SD, Yurchenko AV. 2001. *Ap. J. Suppl. Ser.* 134:181–240
- Kaiser CR, Gunn KE, Brocksopp C, Sokoloski JL. 2004. *MNRAS*. Submitted
- Kaiser CR, Sunyaev R, Spruit HC. 2000 *Astron. Astrophys.* 356:975–88
- King AR. 2004. *MNRAS* 347:L18–20
- Klein-Wolt M, Fender RP, Pooley GG, Belloni T, Migliari S. 2002. *MNRAS* 331:745–64
- Kotani T, Ebisawa K, Dotani T, Inoue H, Nagase F, et al. 2000. *Ap. J.* 539:413–23
- Krolik J.H., ‘Active Galactic Nuclei: from the central black hole to the galactic environment’, Princeton Series in Astrophysics, Princeton, New Jersey, 1999
- Lee JC, Reynolds CS, Remillard R, Schulz NS, Blackman EG, Fabian AC. 2002. *Ap. J.* 567:1102–11
- Levine AM, Bradt H, Cui W, Jernigan JG, Morgan EH, et al. 1996. *Ap. J. Lett.* 469:33–36
- Levinson A, Blandford RD. 1996. *Ap. J.* 456:L29–33

- Lin D, Smith IA, Liang EP, Böttcher M. 2000. *Ap. J. Lett.* 543:141–44
- Livio M, Pringle JE, King AR. 2003. *Ap. J.* 593:184–88
- Maccarone TJ. 2002. *MNRAS* 336:1371–76
- Maccarone TJ, Coppi PS. 2003. *MNRAS* 338:189–96
- Maccarone TJ, Gallo E, Fender R. 2003. *MNRAS* 345:L19–24
- Malzac J, Merloni A, Fabian AC. 2004. *MNRAS*. In press
- Markoff S, Falcke H, Fender RP. 2001. *Astron. Astrophys.* 372:L25–28
- Markwardt CB, Swank JH, Taam RE. 1999. *Ap. J. Lett.* 513:37–40
- Marscher AP, Jorstad SG, Gomez JL, Aller MF, Terasranta H, et al. 2002. *Nature* 417:625–27
- Martocchia A, Matt G, Karas V, Belloni T, Feroci M. 2002. *Astron. Astrophys.* 387:215–21
- McClintock JE, Remillard RA. 2004. In *Compact Stellar X-ray Sources*. Cambridge, UK: Cambridge Univ. Press. In press (astro-ph/0306213)
- Meier D. 1999. *Ap. J.* 522:753–66
- Meier D. 2001. *Ap. J.* 548:L9–12
- Meier DL, Koide S, Uchida Y. 2001. *Science* 291:84–92
- Merloni A, Fabian AC, Ross RR. 2000. *MNRAS* 313:193–97
- Merloni A, Heinz S, di Matteo T. 2003. *MNRAS* 345:1057–76
- Migliari S, Belloni T. 2003. *Astron. Astrophys.* 404:283–89
- Mirabel IF, Bandyopadhyay R, Charles PA, Shahbaz T, Rodríguez LF. 1997. *Ap. J.* 477:L45–48
- Mirabel IF, Dhawan V, Chaty S, Rodríguez LF, Marti J, et al. 1998. *Astron. Astrophys* 333:L1–4
- Mirabel IF, Duc PA, Teyssier R, Paul J, Rodríguez LF, et al. 1993b. *IAU Circ. No.* 5830
- Mirabel IF, Duc PA, Rodríguez LF, Teyssier R, Paul J, et al. 1994. *Astron. Astrophys. Lett.* 282:17–20
- Mirabel IF, Rodríguez LF. 1994. *Nature* 371:46–48
- Mirabel IF, Rodríguez LF. 1999. *Annu. Rev. Astron. Astrophys.* 37:409–43
- Mirabel IF, Rodríguez LF, Cordier B, Paul J, Lebrun F. 1992. *Nature* 358:215–17
- Mirabel IF, Rodríguez LF, Marti J, Teyssier R, Paul J, Auriere M. 1993a. *IAU Circ. No.* 5773
- Mirabel IF, Rodríguez LF, Chary S, Sauvage M, Gerard E, et al. 1996. *Ap. J.* 472:L111–14
- Mitsuda K, Inoue H, Koyama K, Makishima K, Matsuoka M, et al. 1984. *Publ. ASJ* 36:741–59
- Morgan EH, Remillard RA, Greiner J. 1997. *Ap. J.* 482:993–1010
- Muno MP, Morgan EH, Remillard RA. 1999. *Ap. J.* 527:321–40
- Muno MP, Remillard RA, Morgan EH, Waltman EB, Dhawan V, et al. 2001. *Ap. J.* 556:515–32

- Naik S, Agrawal PC, Rao AR, Paul B, Seetha S, Kasturirangan K. 2001. *Ap. J.* 546:1075–85
- Naik S, Agrawal PC, Rao AR, Paul B. 2002. *MNRAS* 330:487–96
- Naik S, Rao AR. 2000. *Astron. Astrophys.* 362:691–96
- Nandi A, Chakrabarti SK, Vadawale SV, Rao AR. 2001. *Astron. Astrophys.* 380:245–50
- Nayakshin S, Rappaport S, Melia F. 2000. *Ap. J.* 535:798–814
- Nespoli E, Belloni T, Homan J, Miller JM, Lewin WHG, et al. 2003. *Astron. Astrophys.* 412:235
- Ogley RN, Bell B, Fender RP, Pooley GG, Waltman EB. 2000. *MNRAS* 317:158–62
- Ostrowski M, Fürst E. 2001. *Astron. Astrophys.* 367:613–16
- Paciesas WS, Deal KJ, Harmon BA, Zhang SN, Wilson CA, et al. 1996. *Astron. Astrophys. Suppl.* 120:205–208
- Paul B, Agrawal PC, Rao AR, Vahia MN, Yadav JS, et al. 1997. *Astron. Astrophys. Lett.* 320:37–40
- Podsiadlowski P, Rappaport S, Han Z. 2003. *MNRAS* 341:385–404
- Pooley GG. 1995. *IAU Circ. No. 6269*
- Pooley GG, Fender RP. 1997. *MNRAS* 292:925–33
- Rau A, Greiner J. 2003. *Astron. Astrophys.* 397:711–22
- Rau A, Greiner J, McCollough ML. 2003. *Ap. J. Lett.* 590:37–40
- Rees MJ. 1978. *MNRAS* 184:P61–65
- Rees MJ, Meszaros P. 1994. *Ap. J.* 430:L93–96
- Reig P, Belloni T, van der Klis M. 2003. *Astron. Astrophys.* 412:229
- Reig P, Belloni T, van der Klis M, Méndez M, Kylafis ND, Ford EC. 2000. *Ap. J.* 541:883–88
- Rodriguez J, Durouchoux P, Mirabel IF, Ueda Y, Tagger M, Yamaoka K. 2002a. *Astron. Astrophys.* 386:271–79
- Rodriguez J, Varnière P, Tagger M, Durouchoux P. 2002b. *Astron. Astrophys.* 387:487–96
- Rodríguez LF, Gerard E, Mirabel IF, Gomez Y, Velasquez A. 1995. *Ap. J. Suppl.* 101:173–79
- Rodríguez LF, Mirabel IF. 1993. *IAU Circ. No. 5900*
- Rodríguez LF, Mirabel IF. 1997. *Ap. J.* 474:L123–25
- Rodríguez LF, Mirabel IF. 1999. *Ap. J.* 511:398–404
- Rothschild RE, Blanco PR, Gruber DE, Heindl WA, MacDonald DR, et al. 1998. *Ap. J.* 496:538–49
- Sams BJ, Eckart A, Sunyaev R. 1996a. *Nature* 382:47
- Sams BJ, Eckart A, Sunyaev R. 1996b. *IAU Circ. No. 6455*
- Sazonov S, Sunyaev R. 1995. *IAU Circ. No. 6209*
- Spada M, Ghisellini G, Lazzati D, Celotti A. 2001. *MNRAS* 325:1559–70

- Stirling AM, Spencer RE, de la Force CJ, Garrett MA, Fender RP, Ogley RN. 2001. *MNRAS* 327:1273–78
- Strohmayer TE. 2001. *Ap. J. Lett.* 554:169–72
- Sunyaev RA, Titarchuk LG. 1980. *Astron. Astrophys.* 86:121–38
- Szuszkiewicz E, Miller JC. 1998. *MNRAS* 298:888–96
- Szuszkiewicz E, Miller JC. 2001. *MNRAS* 328:36–44
- Taam RE, Chen X, Swank JH. 1997. *Ap. J. Lett.* 485:83–86
- Tanaka Y, Lewin WHG. 1995. In *X-ray Binaries*, p. 126. Cambridge, UK: Cambridge Univ. Press.
- Tingay SJ, Jauncey DL, Preston RA, Reynolds JE, Meier DL, et al. 1995. *Nature* 374:141–43
- Tomsick JA, Kaaret P. 2001. *Ap. J.* 548:401–9
- Trudolyubov SP. 2001. *Ap. J.* 558:276–82
- Trudolyubov SP, Churazov EM, Gilfanov MR. 1999a. *Astron. Lett.* 25:718–38
- Trudolyubov SP, Churazov EM, Gilfanov MR. 1999b. *Astron. Astrophys. Lett.* 351:15–18
- van der Klis M. 1995. In *X-ray Binaries*, p. 252. Cambridge, UK: Cambridge Univ. Press
- van der Laan H. 1996. *Nature* 211:1131–33
- Vadawale SV, Rao AR, Chakrabarti SK. 2001. *Astron. Astrophys.* 372:793–802
- Vadawale SV, Rao AR, Naik S, Yadav JS, Ishwara-Chandra CH, et al. 2003. *Ap. J.* 597:1023–35
- Vignarca F, Migliari S, Belloni T, Psaltis D, van der Klis M. 2003. *Astron. Astrophys.* 397:729–38
- Vilhu O, Nevalainen J. 1998. *Ap. J. Lett.* 508:85–89
- Vilhu O, Poutanen J, Nikula P, Nevalainen J. 2001. *Ap. J. Lett.* 553:51–54
- Winkler C, Trams N. 1998. *Astron. Astrophys.* 337:729–38
- Yadav JS, Rao AR, Agrawal PC, Paul B, Seetha S, et al. 1999. *Ap. J.* 517:935–50
- Yu W, Klein-Wolt M, Fender R, van der Klis M. 2003. *Ap. J.* 589:L33–36
- Zampieri L, Turolla R, Szuszkiewicz E. 2001. *MNRAS* 325:1266–74
- Zdziarski AA, Grove JE, Poutanen J, Rao AR, Vadawale SV. 2001. *Ap. J. Lett.* 554:45–48
- Zdziarski AA, Lubinski P, Gilfanov G, Revnivtsev M. 2003. *MNRAS* 342:355–72
- Zhang SN, Harmon BA, Paciesas WS, Fishman GJ. 1995. *IAU Circ. No. 6209*

[Figure 1 about here.]

[Figure 2 about here.]

[Figure 3 about here.]

[Figure 4 about here.]

[Figure 5 about here.]

[Figure 6 about here.]

[Figure 7 about here.]

[Figure 8 about here.]

[Figure 9 about here.]

[Figure 10 about here.]

[Figure 11 about here.]

[Figure 12 about here.]

[Figure 13 about here.]

[Figure 14 about here.]

[Figure 15 about here.]

[Figure 16 about here.]

[Figure 17 about here.]

[Figure 18 about here.]

[Figure 19 about here.]

[Figure 20 about here.]

[Figure 21 about here.]

[Figure 22 about here.]

[Figure 23 about here.]

[Figure 24 about here.]

[Figure 25 about here.]

[Figure 26 about here.]

[Figure 27 about here.]

List of Figures

BATSE 20–100 keV light curve of GRS 1915+105 in 5-day bins. Flux conversion was done with a $\Gamma=2.5$ power-law model (from Harmon et al. 1997). Time ranges from mid-1991 to the launch of <i>RXTE</i>	45
<i>RXTE</i> /ASM light curve, in 1-day bins, from the start of the <i>RXTE</i> mission up to October 12, 2003.	46
<i>RXTE</i> /PCA light curve of GRS 1915+105 from October 7, 1996, with corresponding hardness ratio (13.3–60.0 keV/2.0–13.3 keV) curve (from Belloni et al. 1997a).	47
Upper panel: <i>RXTE</i> /PCA light curve of GRS 1915+105 from June 18, 1997. Middle and lower panels: corresponding inner radius and temperature (from Belloni et al. 1997b).	48
Correlation between total length of a hard event and maximum inner radius of the disc from the data shown in Figure 4. The line is the best fit with a power-law with fixed index 3.5 (from Belloni et al. 1997b).	49
GRS 1915+105 in the kT_{in} - Γ plane for the <i>RXTE</i> /PCA observation of September 9, 1997 (from Markwardt, Swank & Taam 1997). Different symbols correspond to different timing behavior. The gray bands divide the plot into three sections, corresponding to the three states defined by the authors.	50
Sample <i>RXTE</i> /PCA 1-s light curves for six of the 12 classes defined in Belloni et al. (2000).	51
Schematic PCA color-color diagram showing the basic A/B/C states and their observed transitions. The X-ray colors are defined in the following way. HR1 is the ratio of the counts in the 5–13 keV band over those in the 2–5 keV band. HR2 is the ratio 13–60 keV over 2–5 keV. From Belloni et al. (2000).	52
Inner disc temperature versus inner disc radius for two intervals of instability of a representative class- β observation of GRS 1915+105. The lines indicate two levels of constant accretion rate (increasing in the direction of the arrow (from Migliari & Belloni 2003).	53
(a) OSSE spectra of GRS 1915+105 deconvolved with a power-law model. The spectrum labeled 813 corresponds to the probable B state observation. (b) Average of the above with power-law best fit. From Zdziarski et al. (2001).	54
Combined <i>RXTE</i> PCA+HEXTE and INTEGRAL ISGRI+SPI spectra of GRS 1915+105 during a plateau period on April 2, 2003. The inset shows a PCA power density spectrum typical of C state.	55
Residuals for one of the BeppoSAX observation intervals showing the presence of a broad skewed emission line (from Martocchia et al. 2002).	56
Top panel: PCA light curve from October 31, 1997 (class β) with 2-s bin size. Bottom panel: corresponding spectrogram (in logarithmic gray scale). Black corresponds to high power values.	57
Left panel: PDS of two PCA observations from plateau periods. Filled circles are from August 14, 2000; open circles from July 23, 1996 (adapted from Trudolyubov 2001). Right panel: two examples at a higher QPO frequency (<i>open circles</i> : August 18, 1996; <i>filled circles</i> : October 23, 1996).	58

Phase lags associated to a sample of radio-loud plateaux observations of GRS 1915+105 (from Reig et al. 2000). Top panel: phase lags at the QPO frequency. Bottom panel: phase lags of the continuum between 0.1 and 5 Hz. Positive lags correspond to the hard flux lagging the soft flux.	59
Average power density spectrum of the five PCA observations in 1997 when high-frequency QPOs were detected. Both the 40 Hz and the 69 Hz peaks are visible (from Strohmayer 2001).	60
Representative PDS for the three states of GRS 1915+105. A-short refers to short intervals of state A. AB is from a smooth A–B transition during class β (from Reig et al. 2003).	61
Major (superluminal) relativistic ejections from GRS 1915+105. The left panel shows VLA observations over a period of \sim one month in 1994, from Mirabel & Rodríguez (1994). The right panel shows higher-resolution MERLIN imaging over a period of \sim 12 days in 1997, from Fender et al. (1999a).	62
A plateau state in GRS 1915+105, from Fender et al. (1999). The top panel shows radio monitoring at three frequencies, from the Green Bank Interferometer (GBI) and Ryle Telescope (RT). The plateau phase lasts from approximately MJD 50730 to MJD 50750, and is associated with a flat radio spectrum (<i>middle panel</i>). The plateau is associated with steady X-ray emission (<i>lower panel</i>), which has a hard spectrum (state C). Prior to the plateau is a small medium strength optically thin flare (preplateau flare in Klein-Wolt et al. 2002), and following the plateau is a larger optically thin flare (postplateau flare), which in this case was directly resolved into a relativistic ejection event (tickmarks indicate the epochs of the MERLIN observations presented in the of Figure 18). Following the first postplateau flare was a period of four days of X-ray dip/radio oscillation cycles, indicated as QPO. Other occasions of plateaux have resolved the flat-spectrum radio emission into a steady jet such as those presented in Figure 20.	63
Compact core jet associated with the plateau—steady, hard X-ray and radio emission—state in GRS 1915+105 in April 2003 (adapted from Fuchs et al. 2003b). A similar jet in a plateau state in 1998 was reported by Dhawan et al. (2000).	64
Simultaneous radio and X-ray observations of GRS 1915+105 in 1996, from Pooley & Fender (1997). Despite the patchy X-ray coverage there is a clear hint of an association between the semiregular X-ray dipping behavior and the radio oscillations.	65
Simultaneous X-ray and IR observations of GRS 1915+105 in August 1997, from Eikenberry et al. (1998a).	66
X-ray/IR/radio light curve of GRS 1915+105 during a hard X-ray dip, from Mirabel et al. (1998). The radio event is certainly associated with the cycle, and the IR precedes it by \sim 20 min—probably indicating that the IR is synchrotron emission from much closer to the base of the jet than the radio. Note the spike in the X-ray light curve at which point the X-ray hardness drops dramatically, and has been suggested by Mirabel et al. (1998) as the time of launch of the relativistic jet.	67

- Orbital parameters of GRS 1915+105 from IR spectroscopy (Greiner et al. 2001).
 The top panel shows the most likely orbital period, of 33.5 days, for the binary. The lower panel shows the radial velocity data folded on this orbital period. From these data a mass function—corresponding to an absolute lower limit on the mass of the accreting object—of $9.5 \pm 3.0 M_{\odot}$ can be derived. Assuming a companion mass of $\sim 1.2 M_{\odot}$ and an orbital inclination equal to the angle the jets make with the line of sight, i.e., $\sim 70^{\circ}$, then Greiner et al. estimate a mass of $14 \pm 4 M_{\odot}$ for the black hole. 68
- Jet power as a function of Eddington-scaled luminosity for X-ray binaries (*open triangles*) and AGN (*solid squares*), adjusted for the mass term of Merloni, Heinz & di Matteo (2003); from Maccarone, Gallo & Fender (2003). The reduction in radio power in the approximate range 1%–10% Eddington is well-known in X-ray binaries as the quenching of the jet in soft X-ray states, a phenomenon that may also therefore occur in AGN. The data for GRS 1915+105 lie in the most luminous bin, corresponding to FR II-type AGN. . 69
- Possible analogous disc-jet coupling in the AGN 3C 120, from Marscher et al. 2002 70
- A schematic illustrating our model for the evolution of outbursts and related phases of jet formation in GRS 1915+105 and other accreting black holes. Typical X-ray binary outbursts follow the path of the solid arrows, transiting from the canonical LS to the canonical HS via a monotonically softening VHS/IS. This evolution corresponds to leftward motion across the hardness-intensity diagram (*top panel*). We suggest that above some hardness a jet is produced, below that hardness the jet is suppressed, and that close to the transition (indicated by the vertical line) the jet velocity increases to significantly relativistic values (*lower panel*). This line may correspond to the geometrically thin accretion disc reaching the innermost stable circular orbit around the black hole. As a result, crossing the vertical line from left to right results in a shock in the outflow and subsequent cessation of core jet production; this is observed as a singular optically thin radio event. GRS 1915+105 seems to be semicontinuously located in the upper-left region of the diagram, repeatedly crossing the vertical line, producing optically thin radio flares each time it does so. A loop, such as that indicated by the circle, may correspond to a single oscillation event. Extended plateau phases correspond to excursions towards the canonical LS, but are inevitably terminated by a softening and major radio event as the source crosses the vertical line once more. This model seems to be consistent with the behavior of other black hole XRBs, and may even be applicable to AGN. 71

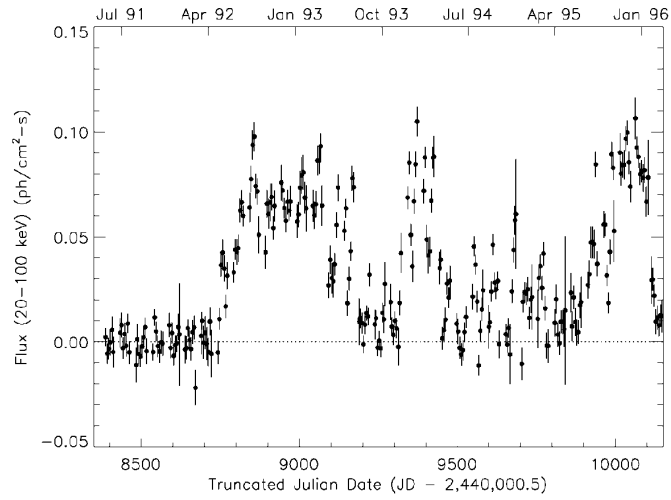


Figure 1: BATSE 20–100 keV light curve of GRS 1915+105 in 5-day bins. Flux conversion was done with a $\Gamma=2.5$ power-law model (from Harmon et al. 1997). Time ranges from mid-1991 to the launch of *RXTE*.

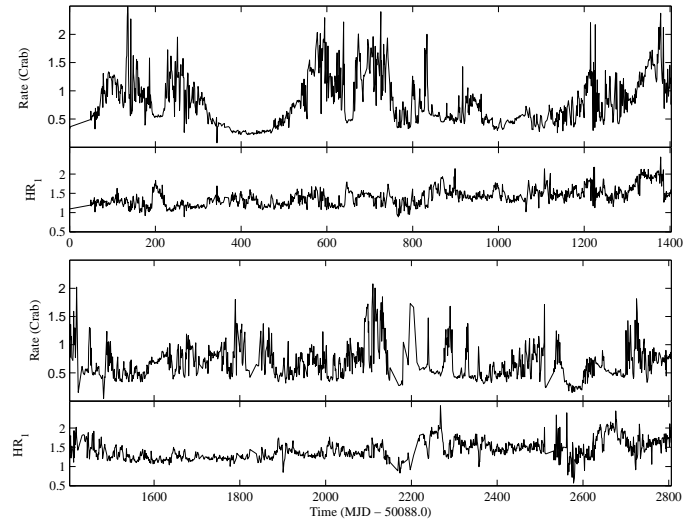


Figure 2: *RXTE*/ASM light curve, in 1-day bins, from the start of the *RXTE* mission up to October 12, 2003.

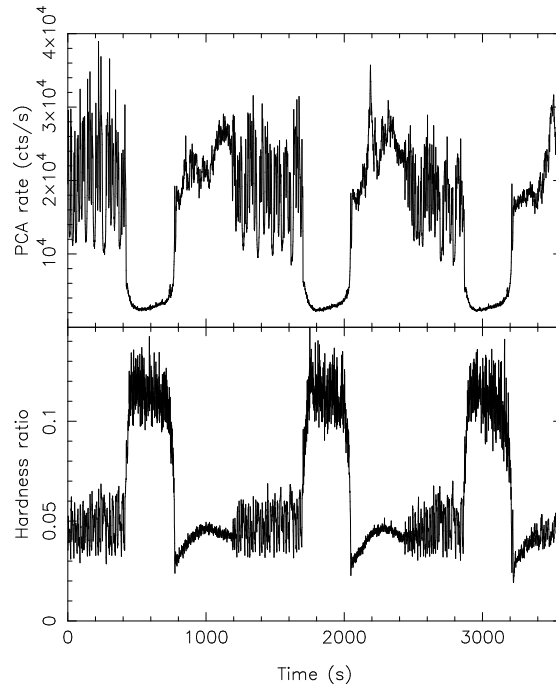


Figure 3: *RXTE*/PCA light curve of GRS 1915+105 from October 7, 1996, with corresponding hardness ratio (13.3–60.0 keV/2.0–13.3 keV) curve (from Belloni et al. 1997a).

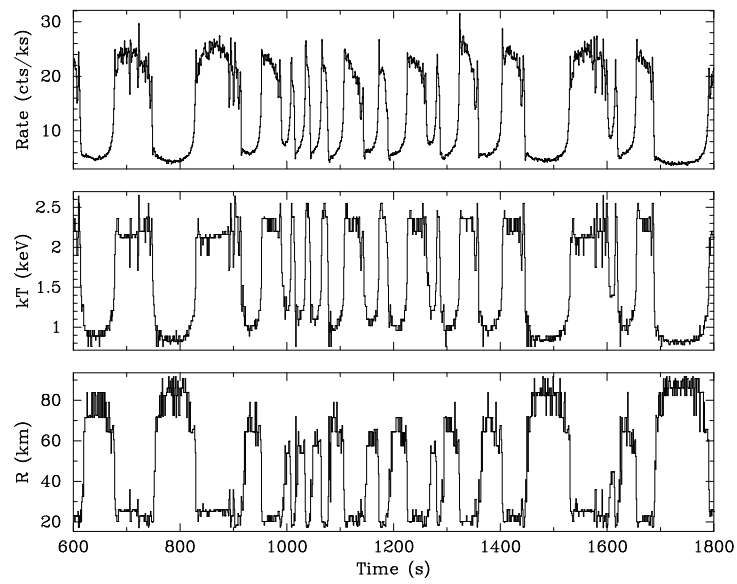


Figure 4: Upper panel: *RXTE*/PCA light curve of GRS 1915+105 from June 18, 1997. Middle and lower panels: corresponding inner radius and temperature (from Belloni et al. 1997b).

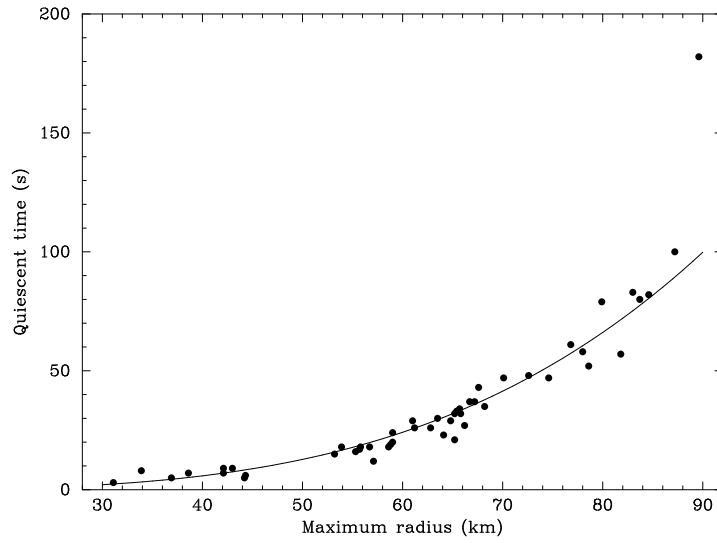


Figure 5: Correlation between total length of a hard event and maximum inner radius of the disc from the data shown in Figure 4. The line is the best fit with a power-law with fixed index 3.5 (from Belloni et al. 1997b).

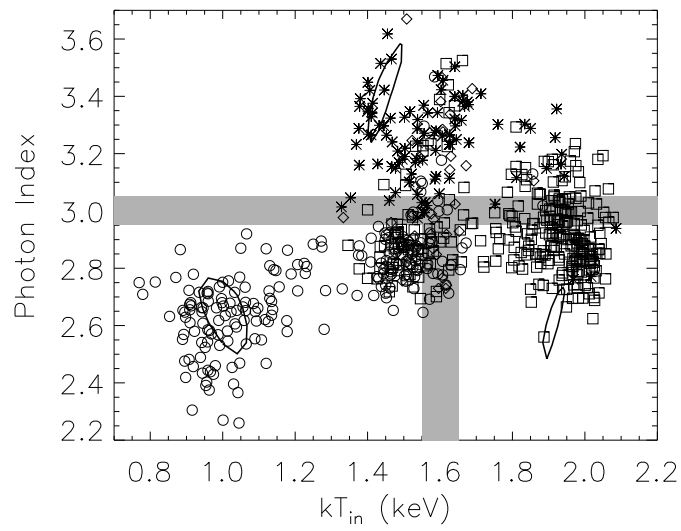


Figure 6: GRS 1915+105 in the kT_{in} - Γ plane for the *RXTE*/PCA observation of September 9, 1997 (from Markwardt, Swank & Taam 1997). Different symbols correspond to different timing behavior. The gray bands divide the plot into three sections, corresponding to the three states defined by the authors.

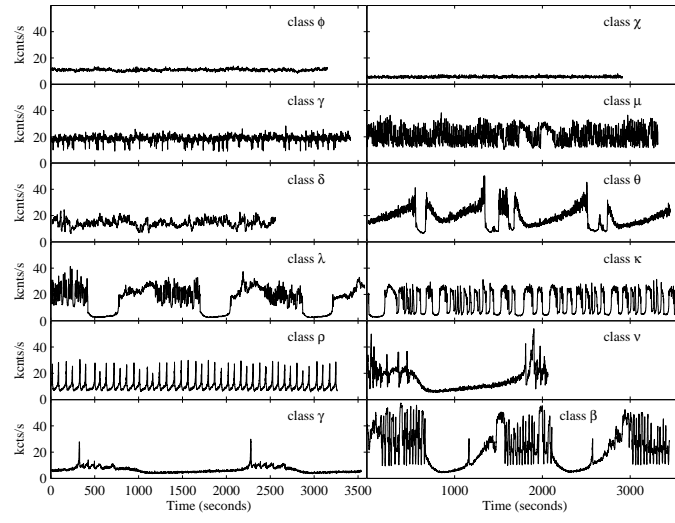


Figure 7: Sample *RXTE*/PCA 1-s light curves for six of the 12 classes defined in Belloni et al. (2000).

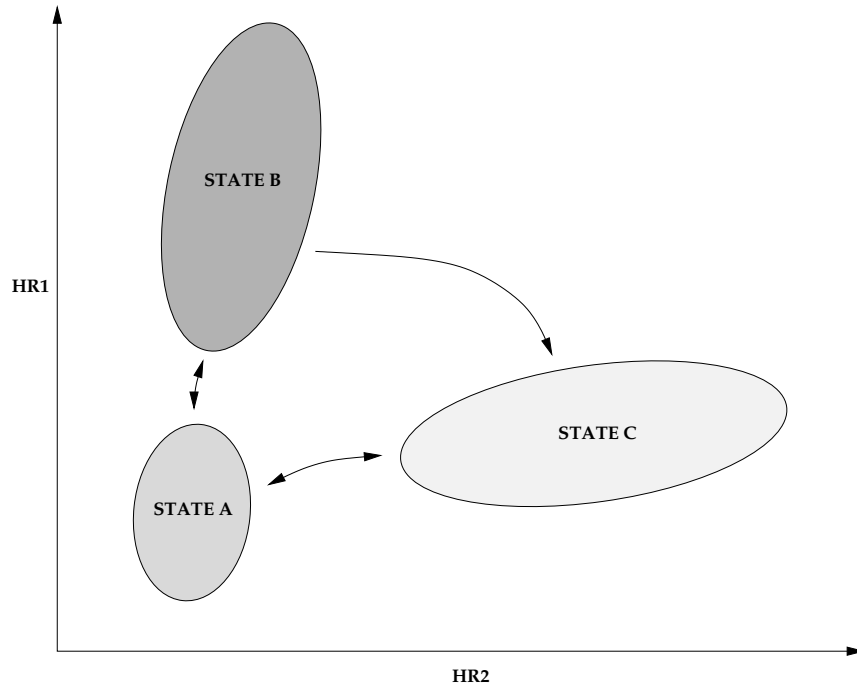


Figure 8: Schematic PCA color-color diagram showing the basic A/B/C states and their observed transitions. The X-ray colors are defined in the following way. HR1 is the ratio of the counts in the 5–13 keV band over those in the 2–5 keV band. HR2 is the ratio 13–60 keV over 2–5 keV. From Belloni et al. (2000).

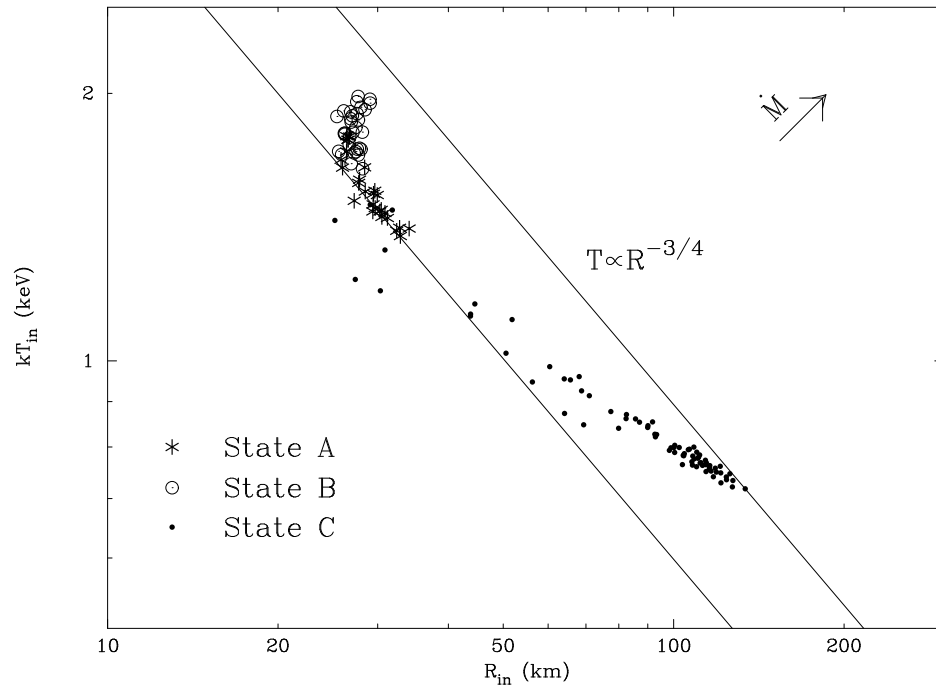


Figure 9: Inner disc temperature versus inner disc radius for two intervals of instability of a representative class- β observation of GRS 1915+105. The lines indicate two levels of constant accretion rate (increasing in the direction of the arrow (from Migliari & Belloni 2003)).

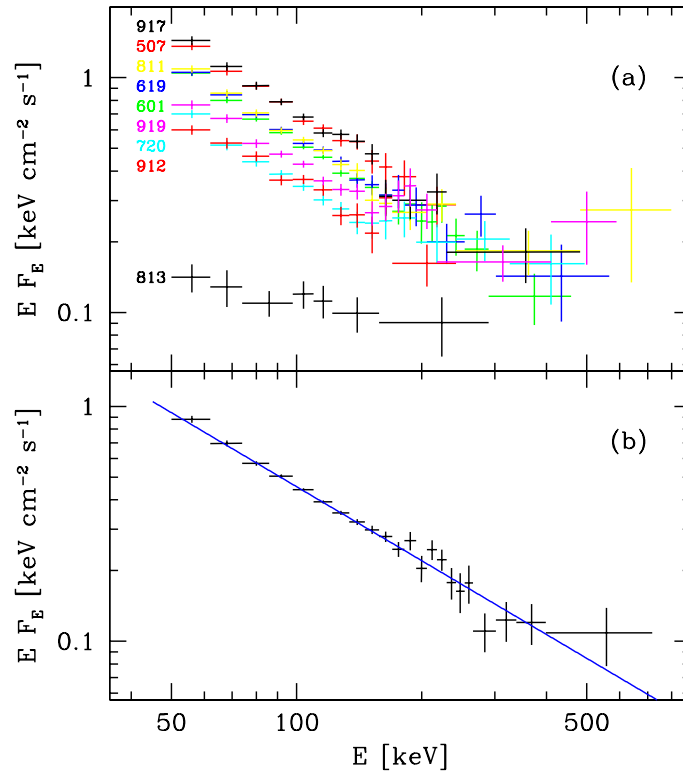


Figure 10: (a) OSSE spectra of GRS 1915+105 deconvolved with a power-law model. The spectrum labeled 813 corresponds to the probable B state observation. (b) Average of the above with power-law best fit. From Zdziarski et al. (2001).

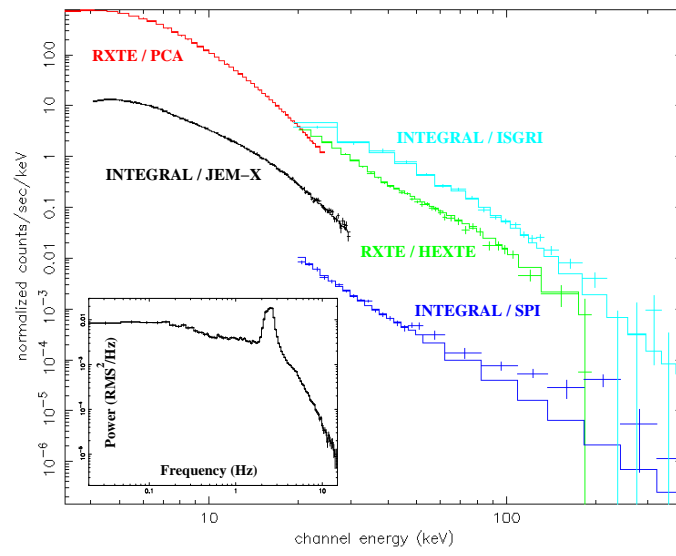


Figure 11: Combined *RXTE* PCA+HEXTE and INTEGRAL ISGRI+SPI spectra of GRS 1915+105 during a plateau period on April 2, 2003. The inset shows a PCA power density spectrum typical of C state.

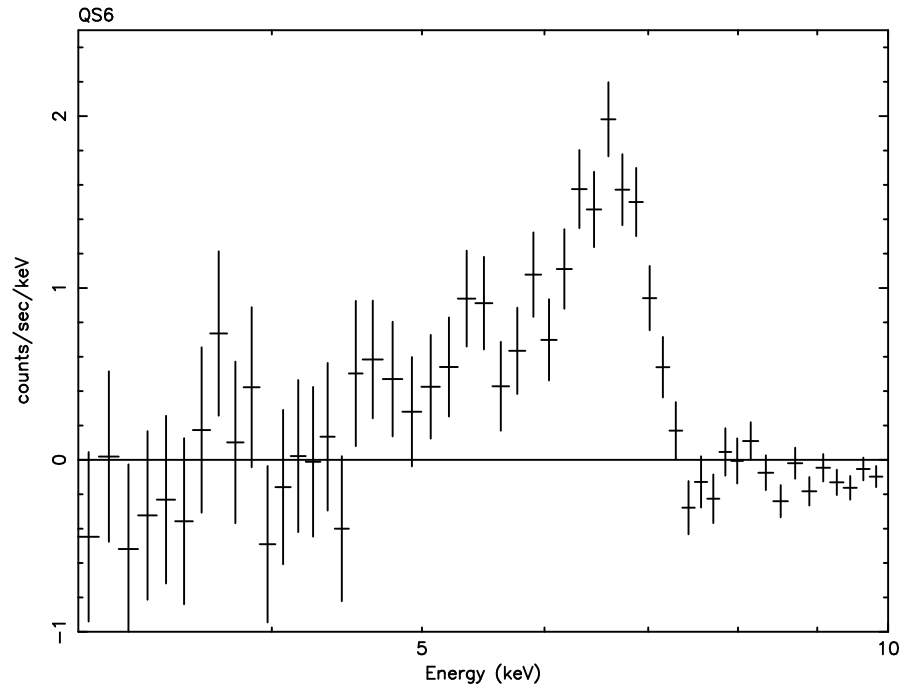


Figure 12: Residuals for one of the BeppoSAX observation intervals showing the presence of a broad skewed emission line (from Martocchia et al. 2002).

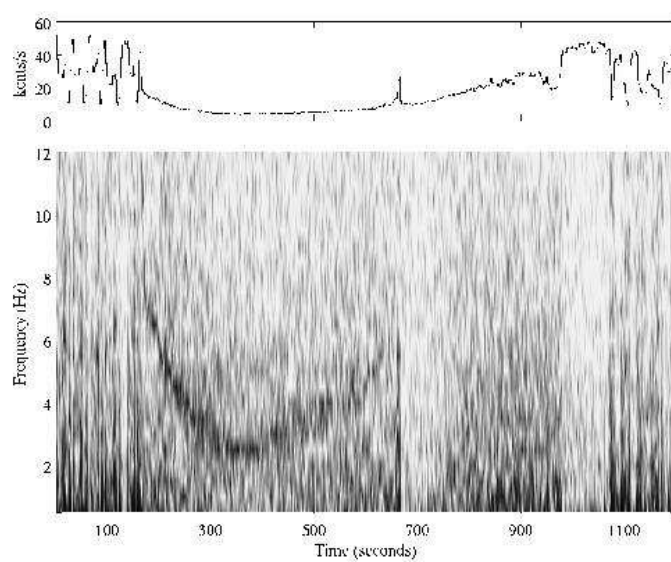


Figure 13: Top panel: PCA light curve from October 31, 1997 (class β) with 2-s bin size. Bottom panel: corresponding spectrogram (in logarithmic gray scale). Black corresponds to high power values.

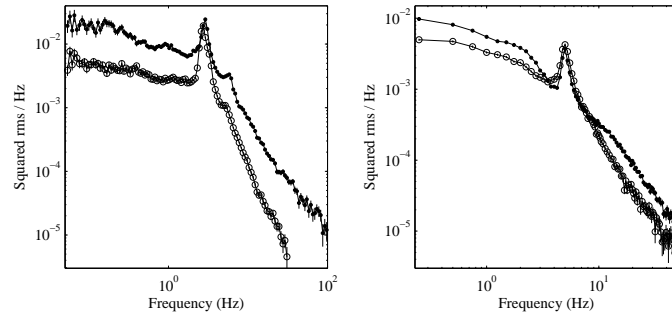


Figure 14: Left panel: PDS of two PCA observations from plateau periods. Filled circles are from August 14, 2000; open circles from July 23, 1996 (adapted from Trudolyubov 2001). Right panel: two examples at a higher QPO frequency (*open circles*: August 18, 1996; *filled circles*: October 23, 1996).

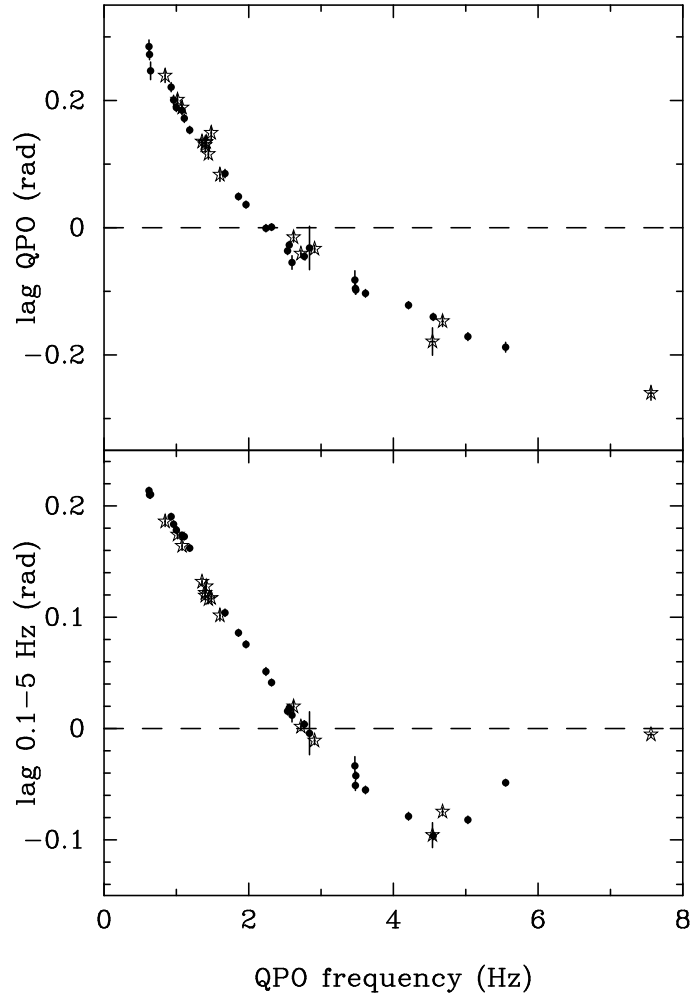


Figure 15: Phase lags associated to a sample of radio-loud plateau observations of GRS 1915+105 (from Reig et al. 2000). Top panel: phase lags at the QPO frequency. Bottom panel: phase lags of the continuum between 0.1 and 5 Hz. Positive lags correspond to the hard flux lagging the soft flux.

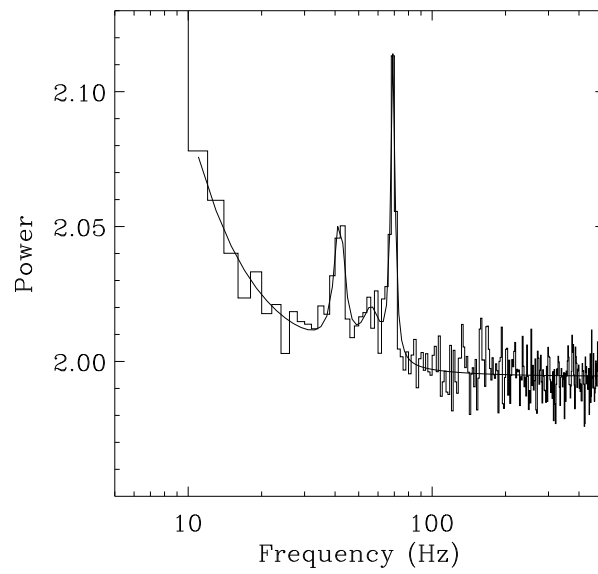


Figure 16: Average power density spectrum of the five PCA observations in 1997 when high-frequency QPOs were detected. Both the 40 Hz and the 69 Hz peaks are visible (from Strohmayer 2001).

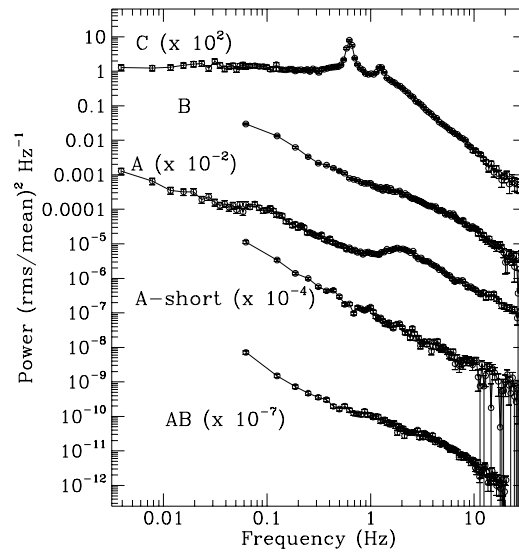


Figure 17: Representative PDS for the three states of GRS 1915+105. A-short refers to short intervals of state A. AB is from a smooth A–B transition during class β (from Reig et al. 2003).

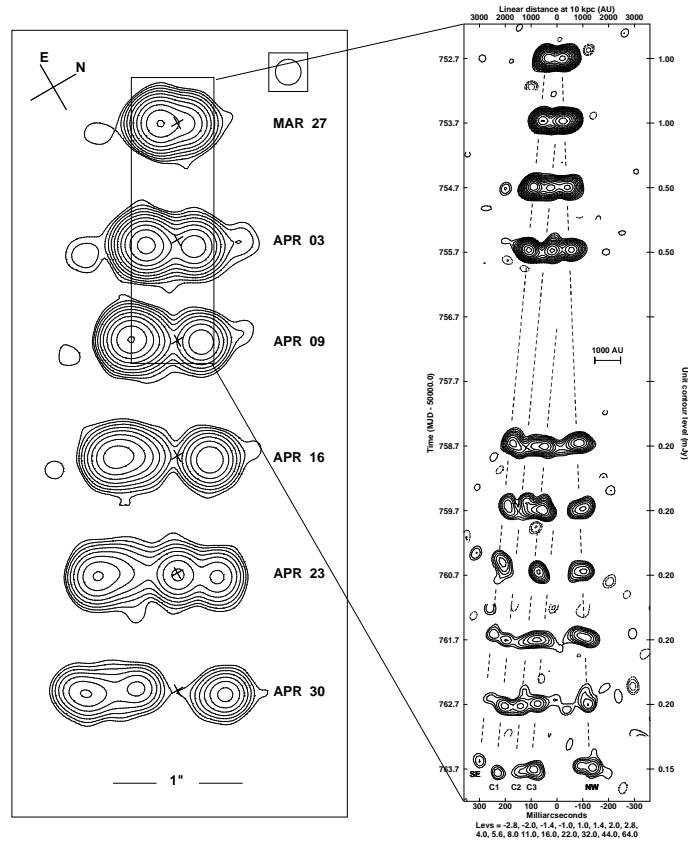


Figure 18: Major (superluminal) relativistic ejections from GRS 1915+105. The left panel shows VLA observations over a period of \sim one month in 1994, from Mirabel & Rodríguez (1994). The right panel shows higher-resolution MERLIN imaging over a period of \sim 12 days in 1997, from Fender et al. (1999a).

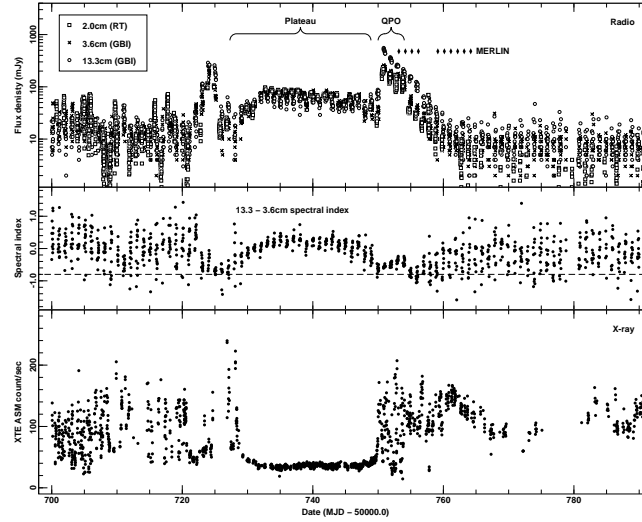


Figure 19: A plateau state in GRS 1915+105, from Fender et al. (1999). The top panel shows radio monitoring at three frequencies, from the Green Bank Interferometer (GBI) and Ryle Telescope (RT). The plateau phase lasts from approximately MJD 50730 to MJD 50750, and is associated with a flat radio spectrum (*middle panel*). The plateau is associated with steady X-ray emission (*lower panel*), which has a hard spectrum (state C). Prior to the plateau is a small medium strength optically thin flare (preplateau flare in Klein-Wolt et al. 2002), and following the plateau is a larger optically thin flare (postplateau flare), which in this case was directly resolved into a relativistic ejection event (tickmarks indicate the epochs of the MERLIN observations presented in the of Figure 18). Following the first postplateau flare was a period of four days of X-ray dip/radio oscillation cycles, indicated as QPO. Other occasions of plateaux have resolved the flat-spectrum radio emission into a steady jet such as those presented in Figure 20.

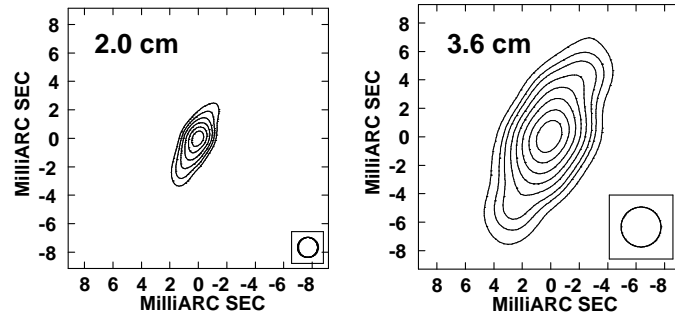


Figure 20: Compact core jet associated with the plateau—steady, hard X-ray and radio emission—state in GRS 1915+105 in April 2003 (adapted from Fuchs et al. 2003b). A similar jet in a plateau state in 1998 was reported by Dhawan et al. (2000).

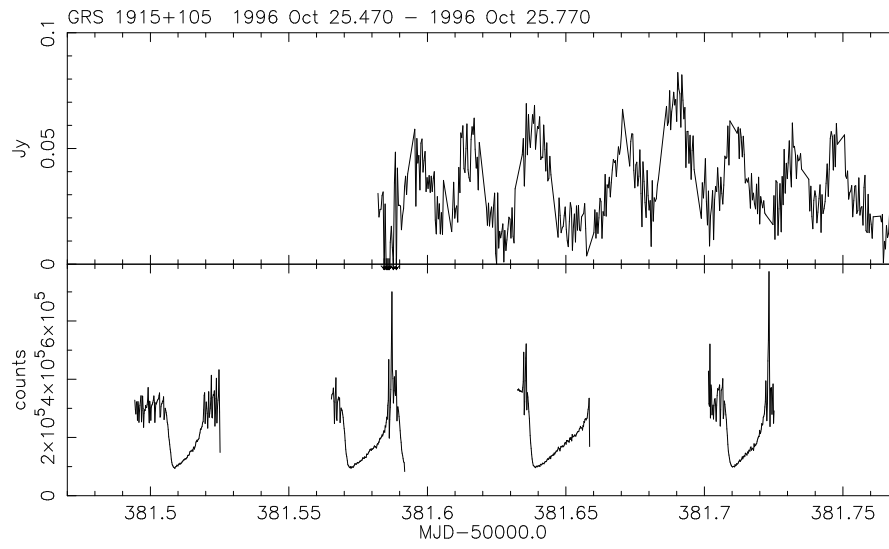


Figure 21: Simultaneous radio and X-ray observations of GRS 1915+105 in 1996, from Pooley & Fender (1997). Despite the patchy X-ray coverage there is a clear hint of an association between the semiregular X-ray dipping behavior and the radio oscillations.

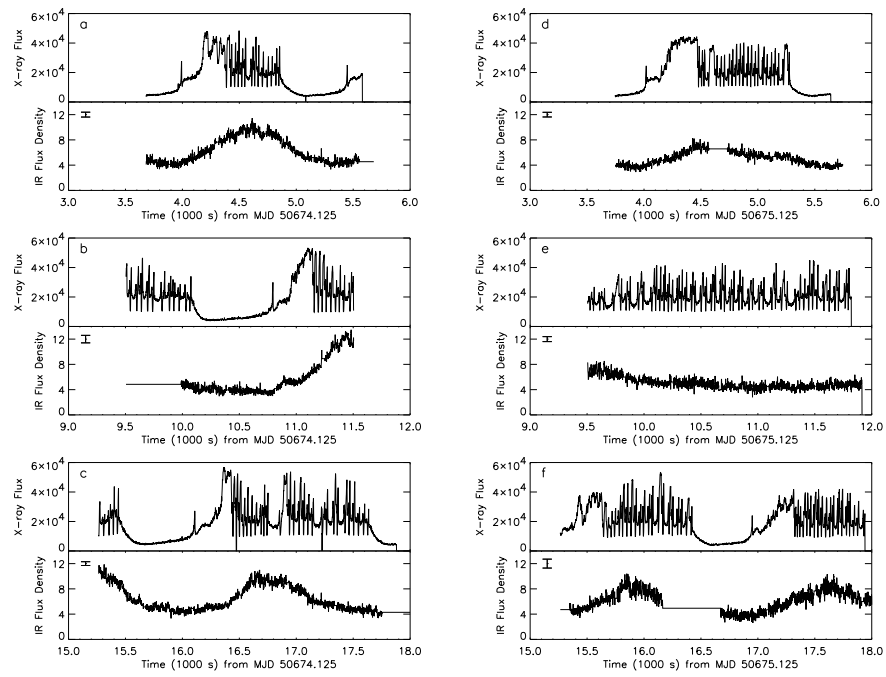


Figure 22: Simultaneous X-ray and IR observations of GRS 1915+105 in August 1997, from Eikenberry et al. (1998a).

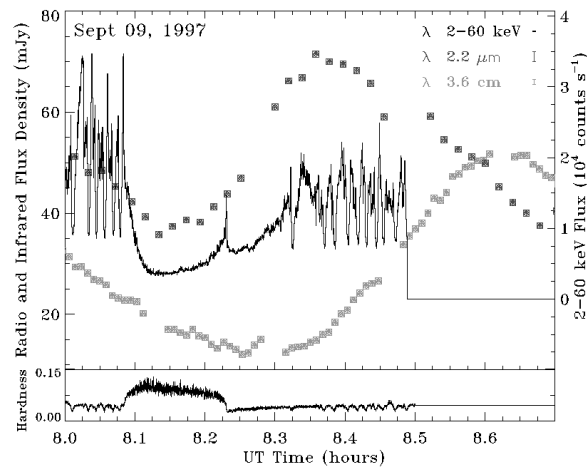


Figure 23: X-ray/IR/radio light curve of GRS 1915+105 during a hard X-ray dip, from Mirabel et al. (1998). The radio event is certainly associated with the cycle, and the IR precedes it by ~ 20 min—probably indicating that the IR is synchrotron emission from much closer to the base of the jet than the radio. Note the spike in the X-ray light curve at which point the X-ray hardness drops dramatically, and has been suggested by Mirabel et al. (1998) as the time of launch of the relativistic jet.

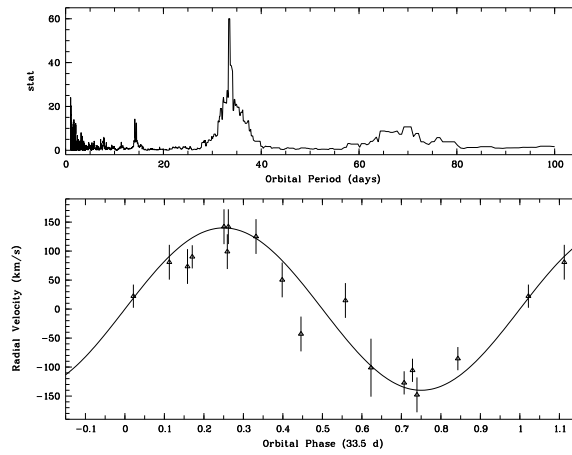


Figure 24: Orbital parameters of GRS 1915+105 from IR spectroscopy (Greiner et al. 2001). The top panel shows the most likely orbital period, of 33.5 days, for the binary. The lower panel shows the radial velocity data folded on this orbital period. From these data a mass function—corresponding to an absolute lower limit on the mass of the accreting object—of $9.5 \pm 3.0 M_{\odot}$ can be derived. Assuming a companion mass of $\sim 1.2 M_{\odot}$ and an orbital inclination equal to the angle the jets make with the line of sight, i.e., $\sim 70^{\circ}$, then Greiner et al. estimate a mass of $14 \pm 4 M_{\odot}$ for the black hole.

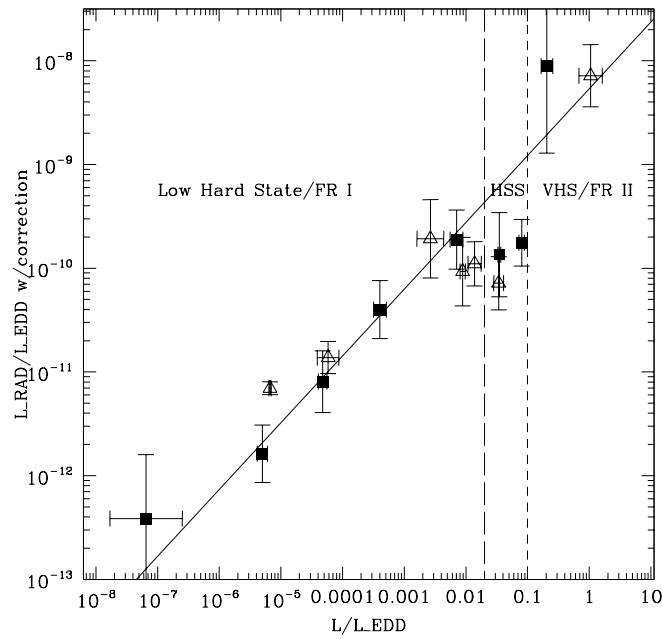


Figure 25: Jet power as a function of Eddington-scaled luminosity for X-ray binaries (*open triangles*) and AGN (*solid squares*), adjusted for the mass term of Merloni, Heinz & di Matteo (2003); from Maccarone, Gallo & Fender (2003). The reduction in radio power in the approximate range 1%–10% Eddington is well-known in X-ray binaries as the quenching of the jet in soft X-ray states, a phenomenon that may also therefore occur in AGN. The data for GRS 1915+105 lie in the most luminous bin, corresponding to FR II-type AGN.

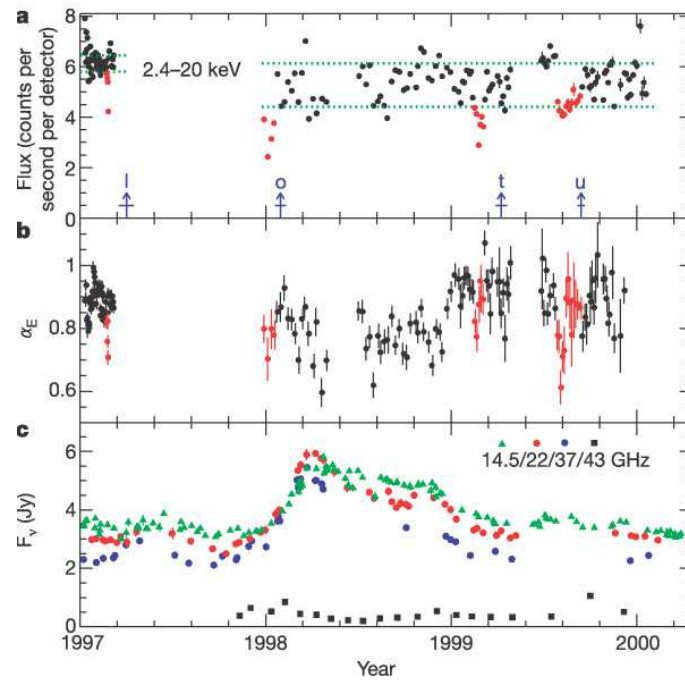


Figure 26: Possible analogous disc-jet coupling in the AGN 3C 120, from Marscher et al. 2002

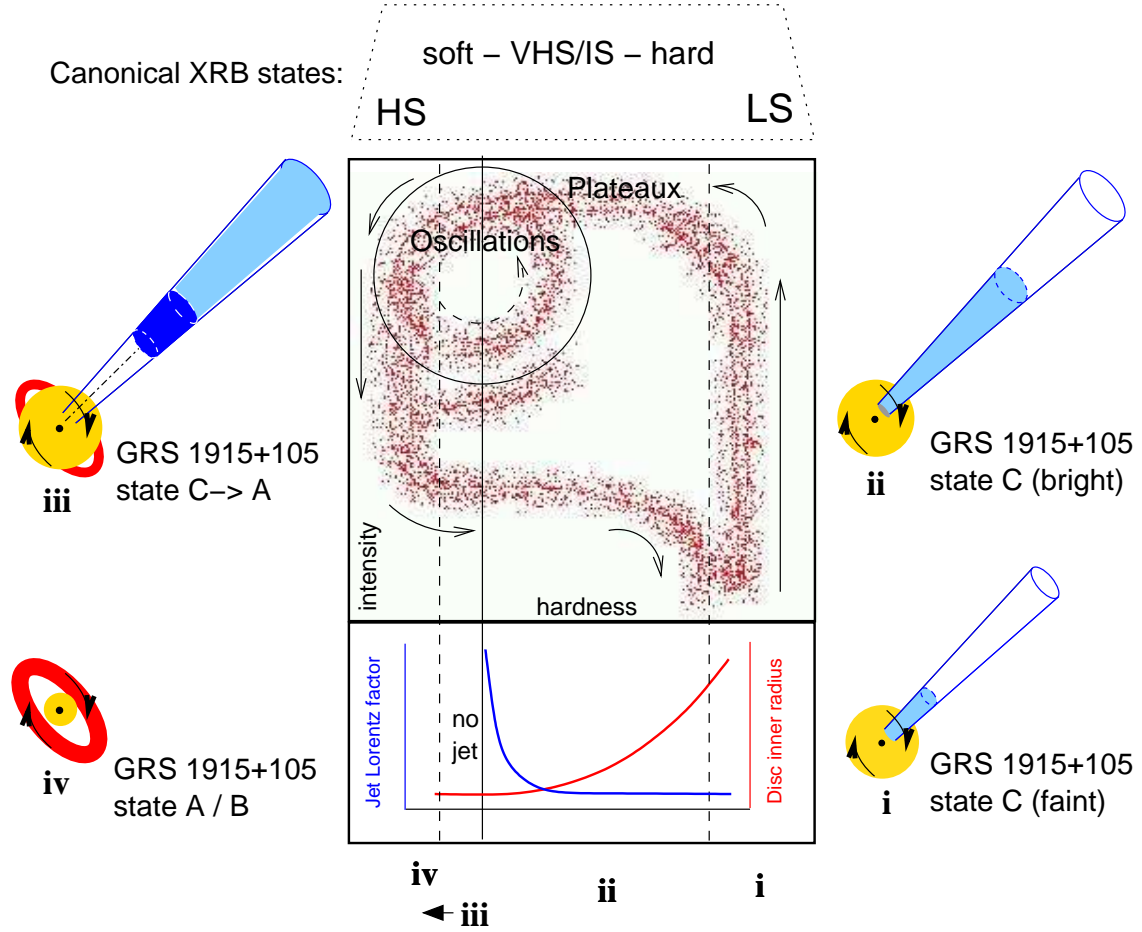


Figure 27: A schematic illustrating our model for the evolution of outbursts and related phases of jet formation in GRS 1915+105 and other accreting black holes. Typical X-ray binary outbursts follow the path of the solid arrows, transiting from the canonical LS to the canonical HS via a monotonically softening VHS/IS. This evolution corresponds to leftward motion across the hardness-intensity diagram (*top panel*). We suggest that above some hardness a jet is produced, below that hardness the jet is suppressed, and that close to the transition (indicated by the vertical line) the jet velocity increases to significantly relativistic values (*lower panel*). This line may correspond to the geometrically thin accretion disc reaching the innermost stable circular orbit around the black hole. As a result, crossing the vertical line from left to right results in a shock in the outflow and subsequent cessation of core jet production; this is observed as a singular optically thin radio event. GRS 1915+105 seems to be semicontinuously located in the upper-left region of the diagram, repeatedly crossing the vertical line, producing optically thin radio flares each time it does so. A loop, such as that indicated by the circle, may correspond to a single oscillation event. Extended plateau phases correspond to excursions towards the canonical LS, but are inevitably terminated by a softening and major radio event as the source crosses the vertical line once more. This model seems to be consistent with the behavior of other black hole XRBs, and may even be applicable to AGN.

List of Tables

Comparison between the properties of the two apparently distinct types of jets produced by GRS 1915+105	73
Schematic comparison between the A/B/C states of GRS 1915+105 and the canon- ical states of BHCs. (adapted from Reig et al. 2003)	74

Table 1: Comparison between the properties of the two apparently distinct types of jets produced by GRS 1915+105

Plateaux jets	Relativistic ejections
Can be steadily produced for up to ~ 20 days	Produced in < 24 h
Optically thick spectrum	Rapidly evolve to an optically thin spectrum
Low polarization ($< 5\%$)	Up to 20% polarization
Some evidence for low velocity	Highly relativistic ($\Gamma > 2$)
Associated with steady hard X-ray (state C) phases	Associated with hard \rightarrow soft X-ray state changes

Table 2: Schematic comparison between the A/B/C states of GRS 1915+105 and the canonical states of BHCs. (adapted from Reig et al. 2003)

Parameter	LS	HS	VHS	State A	State B	State C
kT^a (keV)	< 1	~ 1	1–2	1.8	2.2	0.8
Γ^b	1.5–2	2–3	~ 2.5	~ 3.5	~ 3.1	1.8–2.5
Cutoff ^c	yes	no	no	no	no	no?
Noise ^d	FT	PL	FT & PL	PL	PL	FT
ν_{break}	≤ 1 Hz	-	≥ 1 Hz	1–3 Hz	-	~ 10 Hz
rms	30–50%	$< 3\%$	1–15%	5%–10%	5%–10%	10%–20%
QPO	no	no	1–10 Hz	no	no	1–10 Hz

^aTemperature of the disc blackbody component.

^bPower-law index of the hard spectral component.

^cPresence of a high-energy cutoff.

^dType of noise in the PDS: FT stands for flat-top and PL for power-law.